Preliminary anticancer evaluation of new Pd(II) complexes bearing NNO donor ligands

Shazia Hussain [a], Shabeeb Hussain [a], M. Naveed Zafar [a,*], Irfan Hussain [b], Faizullah Khan [c], Ehsan Ullah Mughal [d], Muhammad Nawaz Tahir [e]

[a] Department of Chemistry, Quaid-i-Azam University, Islamabad 45320, Pakistan
[b] Center of Regenerative Medicine and Stem Cell Research, Aga Khan 74800, University Karachi, Pakistan
[c] Natural and Medical Sciences Research Center, University of Nizwa, Nizwa 616, Sultanate of Oman and Department of Pharmacy, Abdul Wali Khan University Mardan, Mardan 23200, Khyber Pakhtunkhwa, Pakistan
[d] Department of Chemistry, University of Gujrat, Gujrat 50700, Pakistan
[e] Department of Physics, University of Sargodha, 40100 Sargodha, Pakistan

ARTICLE INFO

ABSTRACT

In this study we presented a novel series of NNO tridentate ligands generating imino, amido and oxo donor pocket for Pd(II) coordination. All the compounds were meticulously characterized by elemental analysis and advanced spectroscopic techniques, including FTIR, proton and carbon NMR. The synthesized compounds underwent rigorous evaluation for their potential as anti-cancer agents, utilizing the aggressive breast cancer cell lines MDA-MB (ATCC) and MCF-7 as a crucial model for assessing growth inhibition in cancer cells. Remarkably, the MTT assay unveiled the robust anti-cancer activity for all palladium complexes against MDA-MB-231 and MCF-7 cells. Particularly, complex $[Pd(L^1)(CH_3CN)]$ exhibited exceptional potency with an IC_{50} value of 25.50 ± 0.30 μM (MDA-MB-231) and 20.76 ± 0.30 μM (MCF-7), compared to respective 27.00 ± 0.80 μM and 24.10 ± 0.80 μM for cisplatin, underscoring its promising therapeutic potential. Furthermore, to elucidate the mechanistic basis for the anti-cancer effects, molecular docking studies on tyrosine kinases, an integral target in cancer research, were carried out. The outcome of these investigations further substantiated the remarkable anticancer properties inherent to these innovative compounds. This research offers a compelling perspective on the development of potent anti-cancer agents rooted in the synergy between ligands and Pd(II) complexes and presenting a promising avenue for future cancer therapy endeavors.

1. Introduction

Breast cancer represents a formidable global health challenge, exerting a significant toll on women's well-being and mortality. Its prevalence varies markedly across regions, with a projected impact of around two million cases in 2023, leading to approximately half a million deaths worldwide (de Miguel and Calvo, 2020). The emergence of breast cancer is rooted in the disruption of complex cellular communication pathways within mammary epithelial cells (Boshuizen and Peeper, 2020) Within the tumor microenvironment, a convergence of growth factors and chemokines initiates intricate signaling cascades, driving cancer progression(Huang et al., 2021). These molecular signals interact with a diverse array of receptors, including Receptor Tyrosine

Kinases (RTKs)(Dudani et al., 2019). As single-pass transmembrane proteins, RTKs are widely expressed in the tumor microenvironment and beyond (Arpino et al., 2008). This heightened RTK presence corresponds to increased cancer aggressiveness and reduced overall and disease-free survival rates (Guillen et al., 2018). As we delve into the multifaceted landscape of breast cancer progression and therapeutic strategies, the interplay of RTKs, innovative agents, and historical context intertwines to present an intriguing frontier for advancements in breast cancer management.

Interest in inorganic compounds arose with the discovery of cisplatin, a widely used anticancer agent. Cisplatin along with other platinum drugs such as carboplatin, and oxaliplatin, constitute half of administered anticancer therapies (Chohan and Sumrra, 2010, Emam

et al., 2017, Hussain et al., 2020, Mustafa et al., 2022, Sumrra et al., 2022a, 2022b) However, these agents bring side effects like nausea, hearing loss (Kostova, 2006, Ghani and Mansour, 2011), and organ damage (Dorr, 1996, Zhang et al., 1998, Divsalar et al., 2007, Mansouri-Torshizi et al., 2009, Divsalar et al., 2011). Therefore, development of new anticancer drugs is needed to overcome the problems associated with the already available drugs. Transition metal complexation with some organic reagents including Schiff's bases enhanced their cytotoxicity against cancerous cell (Sumrra et al., 2015, Ejidike and Ajibade, 2016, Abd El-Halim et al., 2018, Ambika et al., 2019). Therefore, the inimitable properties of some transition metal complexes dragged the attention of scientists to synthesize new series of complexes and to test them as anticancer agents (Ferrari et al., 1998, Carotti et al., 2000, Gaccioli et al., 2005, Hussain et al., 2014). Among them, Pd(II) is a good option due to the structural similarity of their complexes with those comprising of Pt(II) and therefore the attention of scientists also dragged toward the coordination compounds of Pd(II) for anticancer investigations (González et al., 1997, Mansouri-Torshizi et al., 2008, Divsalar et al., 2009, Divsalar et al., 2010, Divsalar et al., 2011). Schiff bases, recognized in coordination with palladium metal, amplify the possibilities of complex design and have been used as anticancer agent (Petrović et al., 2015, Tadele and Tsega, 2019, Basaran et al., 2022, Mandal et al., 2022, Rudbari et al., 2022).

In continuation to our previous work on palladium complexes (Zafar et al., 2019, Zafar et al., 2021) in the realm of advancing anticancer therapeutic avenues, eight novel palladium complexes with nitrogen and oxygen donor multidentate proligands were synthesized and successfully characterized using FTIR, elemental analysis, proton and carbon NMR. Single crystal XRD technique helped in identifying successful synthesis of a key amino derivative that proceeded further for the synthesis of proligands and their respective palladium complexes. The anionic amido and neutral imino proligands arms were connected with various groups to study the effect of varying electronic property, hydrophobicity and aromaticity of these new compounds towards their anticancer activity (Fig. 1). Impressively, all metal complexes demonstrated potent inhibitory effects against breast cancer cell lines namely MDA-MB-231 and MCF-7. Notably, **[Pd(L^1)(CH$_3$CN)]** exhibited remarkable potency, displaying an IC$_{50}$ value of (25.50 ± 0.30 μM) and (20.76 ± 0.30). This intricate interplay between ligand design for the synthesis of palladium complexes and compelling anti-cancer potential holds promises for innovative strides in breast cancer management.

An extensive in silico evaluation of palladium complexes, **[Pd(L^1) (CH$_3$CN)]** – **[Pd(L^8)(CH$_3$CN)]**, were carried out to assess their potential as tyrosine kinase inhibitors. The selection of tyrosine kinases as targets for docking studies of synthesized compounds against breast cancer is grounded in their pivotal role in cancer pathogenesis, especially in the context of the heterogeneous breast cancer subtypes (Huang et al., 2020). Tyrosine kinases regulate crucial signaling pathways linked to uncontrolled cell proliferation, a hallmark of cancer, making them pertinent druggable targets for structure-based drug design (Makker et al., 2019). The personalized medicine trend in breast cancer treatment further justifies this choice, allowing tailored therapies that target specific molecular aberrations (Oaknin et al., 2020). Additionally, tyrosine kinase inhibitors can be used in combination with other therapies, potentially leading to synergistic effects and reduced drug resistance (Drilon et al., 2017). Furthermore, the precision of these inhibitors minimizes side effects on normal cells, enhancing patient well-being (Drilon et al., 2017, Huang et al., 2020).

2. Material and methods

2.1. Materials

All the reactions were carried out under inert environment of nitrogen. The solvents used were distilled and purified. All reagents consumed were obtained from commercial sources. 2-chloro-3-nitropyridine (Macklin), cyclohexyl amine (Daejung), o-toluidine (Daejung), benzyl amine (Daejung), 10 % palladium-on-charcoal (Aldrich), hydrazine hydrate (Daejung), bisbenzonitrilepalladium(II) chloride (Sigma). All aldehydes (2-hydroxybenzaldehyde 5-bromo-2-hydroxy-benzaldehyde,4-(diethylamino)-2-hydroxybenzaldehyde,2-hydroxy-1-naphthaldehyde) were purchased from (Daejung), sodium acetate base
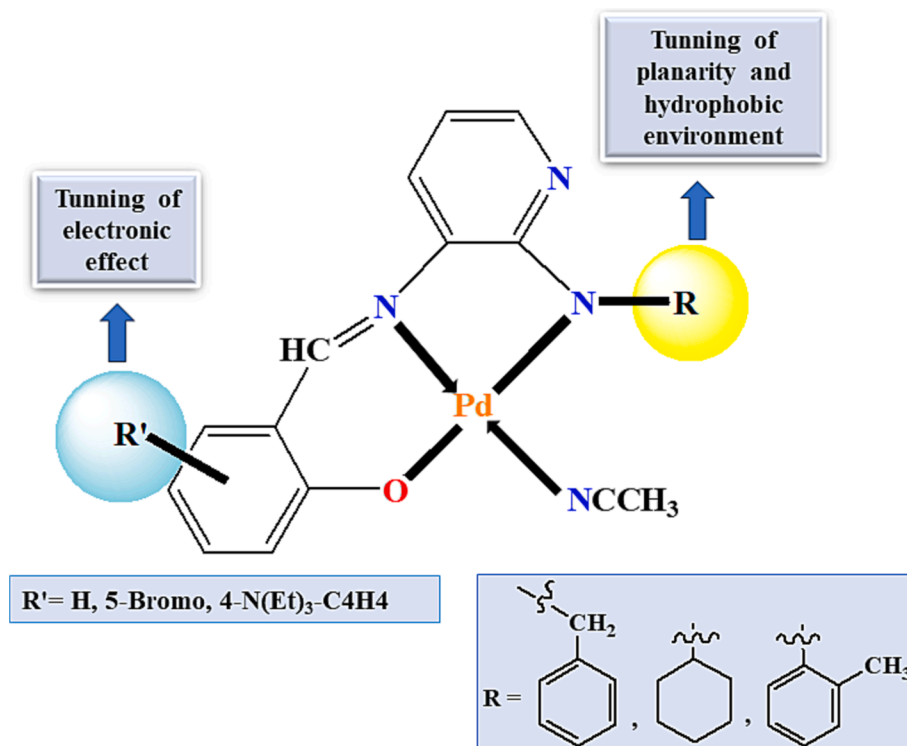

Fig. 1. Design of NNO Donor ligand coordinated Pd(II).

(NaOAc) from Merck. The weights of the reagents were performed by using an electronic balance (Shimadu Corp., Kyoto, Japan). Measurement of melting point of synthesized proligands and complexes were performed by using melting point apparatus (Stuart SMP-10, UK). Bruker micrOTOF QII quadrupole-time-of-flight Mass spectrometer was used to find out the mass of molecular ion peak of respected palladium complexes, elemental analysis for C, H, N were determined from HEJ Research Laboratories, Karachi. ^{1}HNMR and ^{13}CNMR spectra of compounds were obtained using Bruker Advance 300 NMR spectrophotometer, FTIR spectrophotometer (Nicolet Summit Lite, Thermo Scientific USA) was used to record IR spectra of compounds in the range of 4000–400 cm^{-1} and single crystal X-ray studies were performed on Bruker Kappa Apex II X-ray diffractometer.

2.2. Synthesis of proligands

The proligands were synthesized by the following three main steps:

2.2.1. Step 1: Synthesis of Nitro compounds (1–3)

2-chloro-3-nitropyridine was reacted with respective amines (cyclohexylamine, benzyl amine and o-toluidine) in 100 mL round bottomed flask and heated for 1 h at 100° C. The reaction mixture was allowed to cool at room temperature and dissolved in 30 mL ethyl acetate. Afterward, ethyl acetate solution was washed with 30 mL citric acid solution three time and then washed with distilled water. The washed ethyl acetate layer was dried with magnesium sulphate, solvent was removed under reduced pressure resulting in the yellow solid compound which was recrystallized from ethyl acetate/ n-hexane to obtain the pure product.

2.2.1.1. N-benzyl-3-nitropyridin-2-amine (1). Quantities: 2-chloro-3-nitropyridin (500 mg, 3.1 mmol, 1 eq.), benzyl amine (1.0 mL, 9.4 mmol, 3 eq.).

Yield: 90 %, Color: light yellow, M.p: 218–220 °C. FTIR: (KBr, cm^{-1}): 3395 (s), 3079 (m), 3029 (m), 2918 (m), 1722 (m). ^{1}H NMR (300 MHz, (CD$_3$)$_2$SO): δ ppm 8.97 (t, $J = 0.6$ Hz, 1H, —NH), 8.45 (m, 2H, Ar-H),7.33 (m, 5H, Ar-H),) 6.79 (m, 1H, Ar-H), 4.81 (d, $J = 0.6$ Hz 2H, —CH$_2$). ^{13}C NMR (75 MHz, (CD$_3$)$_2$SO): δ ppm 152.9, 148.6, 148.3, 137.5, 128.7, 127.4, 127.0, 120.9, 108.7, 45.9.

2.2.1.2. N-cyclohexyl-3-nitropyridin-2-amine (2). Quantities: 2-chloro-3-nitropyridin (300 mg, 1.9 mmol, 1 eq.), cyclohexyl amine (0.8 mL, 7.5 mmol, 3 eq.).

Yield: 68 %, Color: yellow viscous liquid. FTIR: (KBr, cm^{-1}): 3361 (s), 2932 (s), 2856 (s), 1614 (s). ^{1}HNMR (300 MHz, (CD$_3$)$_2$SO): δ ppm 8.49 (m, 1H, Ar-H), 8.42 (d, 1H, Ar-H), 8.14 (d, $J = 7.8$ Hz, 1H, —NH), 6.77 (m, 1H, Ar-H), 4.19 (m,1H, cy-H), 1.94 (m, 2H, cy-H), 1.70 (m, 3H, cy-H), 1.45 (m, 5H, cy-H). ^{13}CNMR (75 MHz, (CD$_3$)$_2$SO): δ ppm 156.7, 151.7, 135.8, 127.5, 112.3, 49.5, 32.5, 25.5, 24.9. FTIR: (KBr, cm^{-1}): 3361 (s), 2932 (s), 2856 (s), 1614 (s).

2.2.1.3. 3-nitro-N-o-tolylpyridin-2-amine (3). Quantities:2-chloro-3-nitropyridin (500 mg, 3.1 mmol, 1 eq.), o-toluidine (1.0 mL, 9.4 mmol, 3 eq.).

Yield: 86 %, Color: light brown, M.p: 193–195 °C. FTIR: (KBr, cm^{-1}): 3349 (s), 3097 (m), 2925 (m), 2353 (m), 1737 (m). ^{1}HNMR (300 MHz, (CD$_3$)$_2$SO): δ ppm 9.86 (s, 1H, —NH), 8.55 (m, 1H, Ar-H), 8.45 (m, 1H, Ar-H), 7.69 (d, $J = 7.8$ Hz, 1H, Ar-H), 7.30 (d, $J = 7.5$ Hz, 1H, Ar-H), 7.26 (m, 1H, Ar-H), 7.17 (m, 1H, Ar-H), 6.95 (m, 1H Ar-H), 2.23 (s, 3H, —CH$_3$). ^{13}CNMR (75 MHz, (CD$_3$)$_2$SO): δ ppm 155.9, 150.7, 137.4, 135.9, 132.7, 130.4, 128.7, 126.6, 125.9125.8, 114.3, 18.31 (—CH$_3$).

2.2.2. Step II: Synthesis of Amines (4–6)

The nitro containing compounds synthesized in step 1 were then catalytically reduced to NH$_2$ group by using 10 % Pd/C (0.1 g) and hydrazine hydrate (4–5 mL) in 20 mL ethanol. The resulting solution was refluxed for 7–8 h under stirring. The progress of reaction was confirmed by using ethyl acetate and n-hexane (2:3) mixture. When the reduction was completed, the reaction mixture was filtered to remove the 10 % Pd/C catalyst and the dark brown filtrate was then poured into the ice cooled distilled water to obtain dark brown precipitates. Separated the final reduced product by filtration, dried and kept vacuum desiccator.

2.2.2.1. N²-benzylpyridine-2,3-diamine (4). Quantities: N-benzyl-3-nitropyridin-2-amine (1000 mg, 4.3 mmol), reflux time: 7 hrs.

Yield: 65 %, Color: dark brown, M.p: 82–84 °C. FTIR: (KBr, cm^{-1}): 3337 (s), 3233 (m), 3060 (m), 3029 (m), 2922 (m), 2852 (m), 1731 (m). ^{1}HNMR (300 MHz, (CD$_3$)$_2$SO, δ ppm): 7.34 (m, 5H, Ar-H), 7.22 (d, $J = 7.2$ Hz,1H, Ar-H), 6.71 (d, $J = 7.5$ Hz 1H, Ar-H), 6.38 (m, 1H, Ar-H), 6.08 (t, $J = 5.4$ Hz, 1H, –NH), 4.76 (s, 2H, —NH$_2$), 4.57 (d, $J = 5.7$ Hz, 2H, —CH$_2$). ^{13}CNMR (75 MHz, (CD$_3$)$_2$SO, δ ppm): 147.9, 141.6, 135.2, 130.6, 128.5, 127.7, 126.8, 118.0, 113.0, 44.6.

2.2.2.2. N²-cyclohexylpyridine-2, 3-diamine (5). Quantities: N-cyclohexyl-3-nitropyridin-2-amine (1000 mg, 4.5 mmol), reflux time: 8 hrs.

Yield: 68 %, Color: dark green, M.p: 108–110 °C. FTIR: (KBr, cm^{-1}): 3360 (m), 3330 (s), 3131 (m), 2979 (s), 2931 (s), 2852 (s), 2361 (m), 1738 (s). ^{1}H NMR (300 MHz, (CD$_3$)$_2$SO, δ ppm): δ 7.34 (d, $J = 4.8$ Hz 1H, Ar-H), 6.64 (d, $J = 7.2$ Hz, 1H, Ar-H), 6.31 (t, $J = 1.2$ Hz 1H, Ar-H), 5.21 (d, $J = 7.2$ Hz, 1H, —NH), 4.68 (s, 2H, —NH$_2$), 3.36 (11H, Cy-H). ^{13}C NMR (75 MHz, (CD$_3$)$_2$SO, δ ppm): 147.5, 135.2, 130.3, 117.8, 112.2, 49.2, 33.5, 26.1, 25.5.

2.2.2.3. N²-o-tolylpyridine-2,3-diamine (6). Quantities: 3-nitro-N-o-tolylpyridin-2-amine (800 mg, 3.4 mmol), reflux time: 7 hrs.

Yield: 54 %, Color: brown, M.p: 43–45 °C. FTIR: (KBr, cm^{-1}): 3446 (m), 3340 (s), 3226 (m), 3025 (m), 1724 (s). ^{1}HNMR (75 MHz, DMSO, 25 oC, ppm): δ 7.85 (m, 1H, Ar-H), 7.28 (m, 3H, Ar-H), 7.05 (m, 1H, Ar-H), 6.97 (t, $J = 7.5$ Hz, 1H, Ar-H), 6.83 (m, 1H, Ar-H), 6.00 (s, 1H, —NH), 3.47 (s, 2H, —NH$_2$), 2.32 (s, 3H, —CH$_3$). ^{13}CNMR (75 MHz, (CD$_3$)$_2$SO, δ ppm): 145.3, 139.6, 139.0, 131.9, 130.6, 127.1, 126.6, 123.3, 121.9, 118.5, 117.7, 18.0.

2.2.3. Step III: Synthesis of proligands

In 100 mL round bottom flask, aldehyde (1.0 eq.) was dissolved in 10 mL ethanol, 1–2 drops of glacial acetic was added and refluxed the solution for 30–40 min followed by adding 15 mL ethanolic solution of amine (4–6) synthesized in step 2. After 4–5 h of refluxing the color of solution was changed from light orange to yellow. when the reaction was completed, the ethanol was removed by rotary evaporator resulted in the final product which was purified by column chromatography by using n-hexane/ethyl acetate solvent mixture.

2.2.3.1. 2-((2-(benzylamino)pyridin-3-ylimino)methyl)phenol, (H₂L¹). Quantities: N²-benzylpyridine-2,3-diamine (600 mg, 3.0 mmol, 1.0 eq.), 2-hydroxybenzaldehyde (0.31 mL, 3.0 mmol, 1.0 eq.), reflux time: 4 hrs. Eluent: n- hexane/ethyl acetate (90:10 %).

Yield: 55 %, Color: yellow, M.p: 135–137 °C. FTIR: (KBr, cm^{-1}): 3357 (m), 3268 (m), 3045 (m), 2957 (m), 2934 (m), 2842 (m), 1654 (m), 1638 (s), 1581 (m). ^{1}HNMR (300 MHz, (CD$_3$)$_2$SO, δ ppm): 11.96 (s, 1H, —OH), 10.92 (s, 1H, —CH), 8.39 (m, 2H, Ar-H), 8.15 (m, 1H, Ar-H), 7.92 (m, 1H, Ar-H), 7.78 (d, $J = 8.4$ Hz, 1H, Ar-H), 7.44 (m, 4H, Ar-H), 7.08 (t, $J = 3.3$ Hz,1H, Ar-H)), 6.96 (d, $J = 7.8$ Hz 1H, Ar-H)), 6.84 (t, $J = 6$ Hz, 1H, NH) 6.62 (m, 1H, Ar-H), 4.64 (d, 2H, CH$_2$). ^{13}CNMR (75 MHz, (CD$_3$)$_2$SO, δ ppm): δ 164.5, 152.8, 146.2, 141.0, 136.9, 133.3, 132.8, 131.0, 128.1, 127.6, 126.5, 126.0, 124.5, 119.7, 117.8, 112.4, 44.3.

2.2.3.2. 2-((2-(benzylamino)pyridin-3-ylimino)methyl)-4-bromophenol, (H$_2$L^2). Quantities: N^2-benzylpyridine-2,3-diamine (0.50 g, 2.5 mmol, 1 eq.), 5-bromo-2-hydroxybenzaldehyde (0.50 mg, 2.5 mmol, 1 eq.), reflux time: 5 hrs. Eluent: n- hexane/ethyl acetate (80:20 %).

Yield: 62 %, Color: yellow, M.p.: 146–148 °C. FTIR: (KBr, cm^{-1}): 3394 (m), 3375 (m), 3098 (m), 2961 (m), 2917 (m), 2849 (m), 1675 (m), 1614 (s), 1587 (m). ^{1}HNMR (300 MHz, (CD$_3$)$_2$SO, δ ppm): 12.46 (s, 1H, —OH), 8.79 (s, 1H, —CH), 8.02 (m, 1H, Ar-H), 7.45 (d, $J = 6.9$ Hz, 2H, Ar-H), 7.37 (m, 1H, Ar-H,), 7.32 (m, 2H, Ar-H), 7.23 (d, $J = 6.9$ Hz, 2H, Ar-H), 7.11 (m, 1H, Ar-H), 6.93 (t, $J = 7.6$ Hz, 1H, Ar-H), 6.65 (m, 1H, Ar-H), 6.37 (t, $J = 6.3$ Hz, 1H, —NH), 4.81 (d, J$_{HH}$ = 6.3 Hz, 2H, —CH$_2$). ^{13}CNMR (75 MHz, (CD$_3$)$_2$SO, δ ppm): δ 164.2, 152.9, 150.8, 148.4, 146.2, 141.1, 130.9, 128.1, 127.4, 126.5, 124.4, 123.9, 119.8, 118.7, 115.5, 112.4, 44.3.

2.2.3.3. 1-((2-(benzylamino)pyridin-3-ylimino)methyl)naphthalen-2-ol, (H$_2$L^3). Quantities: N^2-benzylpyridine-2,3-diamine (0.50 g, 2.5 mmol, 1.0 eq.), 2-hydroxy-1-naphthaldehyde (0.43 g, 2.5 mmol, 1.0 eq.), reflux time: 4 hrs. Eluent: n- hexane/ethyl acetate (95:5%).

Yield: 61.5 %, Color: yellow, M.p.: 168–170 °C. FTIR: (KBr, cm^{-1}): 3338 (m), 3222 (m), 3058 (m), 2962 (m), 2920 (m), 2849 (m), 1634 (m), 1626 (s), 1572 (m). ^{1}HNMR (300 MHz, (CD$_3$)$_2$SO, δ ppm): 14.68 (s, 1H, —OH), 9.67 (s, 1H, —CH), 8.58 (d, $J = 8.1$ Hz, 1H, Ar-H,), 8.03 (d, $J = 9$ Hz, 1H, Ar-H), 7.96 (d, $J = 4.2$ Hz, 1H, Ar-H), 7.90 (d, $J = 8.1$ Hz, 1H, Ar-H), 7.60 (d, $J = 6.9$ Hz, 2H, Ar-H), 7.43 (t, $J = 7.5$ Hz, 2H, Ar-H), 7.35 (d, $J = 8.1$ Hz, 2H, Ar-H), 7.29 (t, $J = 7.2$ Hz, 3H, Ar-H), 6.85 (t, $J = 5.1$ Hz, 1H, Ar-H), 6.65 (t, $J = 6.9$ Hz, 1H, –NH), 4.65 (d, $J = 8.1$ Hz, 1H, —CH$_2$). ^{13}C NMR (75 MHz, (CD$_3$)$_2$SO, δ ppm): 163.4, 160.6, 152.8, 146.1, 141.5, 135.8, 132.9, 130.5, 129.4, 128.5, 127.8, 127.6, 126.8, 126.2, 124.1, 122.7, 121.4, 120.0, 112.8, 110.5, 44.32.

2.2.3.4. 2-((2-(benzylamino) pyridin-3-ylimino) methyl) −5-(diethylamino)phenol, (H$_2$L^4). Quantities: N^2-benzylpyridine-2,3-diamine (0.55 mg, 2.7 mmol, 1.0 eq.), 4-(diethylamino)-2-hydroxybenzaldehyde (0.53 mg, 2.5 mmol, 1.0 eq.), reflux time: 5hrs. Eluent: n- hexane/ethyl acetate (90:10 %).

Yield: 57.5 %, Color: yellow, Mp: 140–142 °C. FTIR: (KBr, cm^{-1}): 3453 (m), 3364 (m), 3095 (m), 2987 (m), 2932 (m), 2876 (m), 1675 (m), 1645 (s), 1585 (m). ^{1}HNMR (300 MHz, (CD$_3$)$_2$SO, δ ppm): 12.66 (s, 1H, —OH), 8.54 (s, 1H, —CH), 7.92 (m, 1H, Ar-H), 7.43 (d, $J = 7.2$ Hz, 2H, Ar-H), 7.32 (m, 5H, Ar-H), 6.62 (m, 1H, Ar-H), 6.37 (m, 1H, Ar-H), 6.14 (d, $J = 2.4$ Hz, 1H, Ar-H), 6.13 (t, $J = 10.8$ Hz, 1H, —NH), 4.77 (d, $J = 5.7$ Hz, 2H, —CH$_2$), 3.49 (q, $J = 6.9$ Hz, 4H, —CH$_2$), 1.21 (d, $J = 6.9$ Hz, 6H, —CH$_3$). ^{13}CNMR (75 MHz, (CD$_3$)$_2$SO, δ ppm): 163.0, 162.9, 152.9, 152.0, 144.5, 141.2, 134.3, 131.9, 128.9, 127.4, 126.4, 123.5, 112,4, 109.3, 103.9, 97.04, 44.3, 43.9, 12.0.

2.2.3.5. 4-bromo-2-((2-(cyclohexylamino)pyridin-3-ylimino)methyl) phenol, (H$_2$L^5). Quantities used: N^2-cyclohexylpyridine-2,3-diamine (0.50 g, 2.6 mmol, 1.0 eq.), 5-bromo-2-hydroxybenzaldehyde (0.52 g, 2.6 mmol, 1.0 eq.), Reflux time: 3 hrs. Eluent: n- hexane/ethyl acetate (90:10 %).

Yield: 67 %, Color: yellow, Mp: 123–125 °C˙ FTIR: (KBr, cm^{-1}): 3592 (s), 3378 (w), 2870 (m),1731 (m), 1604 (m). ^{1}HNMR (300 MHz, (CD$_3$)$_2$SO, δ ppm): 12.61 (s, 1H, —OH), 8.82 (s, 1H, —CH), 8.02 (d, $J = 4.8$ Hz, 1H, Ar-H), 7.78 (d, $J = 2.7$ Hz, 1H, Ar-H), 7.57 (m, 1H, Ar-H), 7.41 (m, 1H, Ar-H), 6.97 (d, $J = 8.7$ Hz, 1H, Ar-H), 6.64 (m, 1H, Ar-H), 5.47 (d, $J = 7.5$ Hz, 1H, —NH), 3.59 (m, 1H, Cy-H), 1.78 (m, 4H, Cy-H), 1.45 (m, 6H, Cy-H). ^{13}CNMR (75 MHz, (CD$_3$)$_2$SO, δ ppm): 162.7, 159.7, 152.3, 146.5, 135.5, 134.5, 130.2, 124.6, 121.4, 119.0, 111.9, 110.1, 49.2, 32.9, 25.7, 25.0.

2.2.3.6. 2-((2-(cyclohexylamino) pyridin-3-ylimino) methyl)-5-(diethylamino)phenol, (H$_2$L^6). Quantities used: N^2-cyclohexylpyridine-2,3-diamine (0.55 g, 2.8 mmol, 1.0 eq.), 4-(diethylamino)-2-

hydroxybenzaldehyde (0.55 g, 2.8 mmol, 1.0 eq.), Reflux time: 4hrs. Eluent: n- hexane/ethyl acetate (80:20 %).

Yield: 57.5 %, Color: yellow. M.p: 154–156 °C. FTIR: (KBr, cm^{-1}): 3379 (w), 3215 (s), 2922 (m), 2852 (m), 2362 (m), 2340 (m),1734 (m), 1636 (m), 1599 (m). ^{1}HNMR (300 MHz, (CD$_3$)$_2$SO, δ ppm): 12.98 (s, 1H, —OH), 8.53 (s, 1H, CH), 7.91 (d, $J = 6.3$ Hz, 1H, Ar-H), 7.32 (d, $J = 6.5$ Hz, 1H, Ar-H), 7.25 (d, $J = 6.3$ Hz, 1H, Ar-H), 6.58 (m, 1H, Ar-H), 6.39 (m, 1H, Ar-H), 6.16 (d, $J = 2.4$ Hz 1H, Ar-H), 5.23 (d, $J = 6$ Hz,1H, NH), 4.07 (m, 1H, Cy-H), 3.51 (q, $J = 4.2$ Hz, 4H, —CH$_2$), 1.74 (m, 2H, Cy-H), 1.65 (m, 2H, Cy-H), 1.46 (m, 6H, Cy-H), 1.30 (t, $J = 6.3$ Hz, 6H, —CH$_3$). ^{13}CNMR (75 MHz, (CD$_3$)$_2$SO, δ ppm): 163.1, 162.4, 152.4 151.9, 144.7, 134.2, 131.4, 123.1, 111.9, 109.3, 103.9, 97.1, 48.8, 48.7, 44.2, 25.7, 24.9, 12.0.

2.2.3.7. 2-((2-(o-toluidino)pyridin-3-ylimino)methyl)-4-bromophenol, (H$_2$L^7). Quantities: N^2-o-tolylpyridine-2,3-diamine (0.60 g, 3.0 mmol, 1.0 eq.), 5-bromo-2-hydroxybenzaldehyde (0. 60, 3.0 mmol, 1.0 eq.), Reflux time: 4hrs. Eluent: n- hexane/ethyl acetate (92:08 %).

Yield: 71 %, light orange, M.p: 127–129 °C. FTIR: (KBr, cm^{-1}): 3347 (s), 3295(w), 3109 (m), 3017 (m), 2914 (m), 2656 (m),1657 (m), 1623 (m), 1586 (m). ^{1}HNMR (300 MHz, (CD$_3$)$_2$SO, δ ppm): 12.50 (s, 1H, —OH), 8.96 (s, 1H, —CH), 8.26 (d, $J = 7.8$ Hz, 1H, Ar-H), 8.12 (m, 1H, Ar-H), 7.85 (d, $J = 2.4$ Hz, 1H, Ar-H), 7.62 (m, 1H, Ar-H), 7.58 (t, $J = 7.8$ Hz, 1H, Ar-H), 7.36 (s, 1H, —NH), 7.21 (t, $J = 7.8$ Hz, 2H, Ar-H), 6.98 (d, $J = 7.5$ Hz,1H, Ar-H), 6.95 (m, 1H, Ar-H), 6.88 (d, $J = 9$ Hz, 1H, Ar-H) 2.33 (s, 3H, —CH$_3$). ^{13}CNMR (75 MHz, (CD$_3$)$_2$SO, δ ppm): 163.7, 159.7, 150.4, 146.2, 139.0, 135.9, 134.7, 131.4, 130.1, 128.2, 126.2, 122.4, 121.5, 121.1, 120.9, 119.1, 114.8, 110.4, 17.3.

2.2.3.8. 2-((2-(o-toluidino)pyridin-3-ylimino)methyl)-5-(diethylamino) phenol, (H$_2$L^8). Quantities: N^2-o-tolylpyridine-2,3-diamine (0.60 g, 3.0 mmol, 1.0 eq.), 4-(diethylamino)-2-hydroxybenzaldehyde (0. 60, 3.0 mmol, 1.0 eq.), Reflux time: 4hrs. Eluent: n- hexane/ethyl acetate (92:08 %).

Yield: 68 %, light orange, M.p: 137–139 °C. FTIR: (KBr, cm^{-1}): 3365 (s), 3199(w), 3112 (m), 3032 (m), 2923 (m), 2676 (m),1687 (m), 1614 (m), 1564 (m). ^{1}HNMR (300 MHz, (CD$_3$)$_2$SO, δ ppm): 12.98 (s, 1H, —OH), 8.89 (s, 1H, —CH), 8.22 (d, $J = 3.9$ Hz, 1H, Ar-H), 7.81 (d, $J = 4.2$ Hz, 1H, Ar-H), 7.49 (d, $J = 2.4$ Hz, 1H, Ar-H), 7.36 (m, 1H, Ar-H), 7.22 (t, $J = 6$ Hz, 2H, Ar-H), 7.02 (s, 1H, —NH), 6.84 (m, 2H, Ar-H), 6.73 (d, $J = 3.3$ Hz, 1H, Ar-H), 6.47 (m, 1H, Ar-H), 3.37 (q, $J = 4.2$ Hz, 4H, —CH$_2$), 2.39 (s, 3H, —CH$_3$), 2.25 (d, $J = 6.9$ Hz, 6H, —CH$_3$). ^{13}CNMR (75 MHz, (CD$_3$)$_2$SO, δ ppm): 164.3, 160.5, 159.8, 153.7, 149,0, 144.7, 139.7, 136.6, 132.1, 130.2, 129.2, 127.8, 124.4, 123.5, 120.1, 119.8, 115.4, 112.6, 44.7, 17.3, 12.9.

2.3. Synthesis of palladium complexes, [Pd(L^1)(CH$_3$CN)] – [Pd(L^8) (CH$_3$CN)]

In a 50 mL of two necked round bottom flask containing 10 mL dried acetonitrile, PdCl$_2$(PhCN)$_2$ (1.0 equivalent) was added with prior inert atmosphere and heated it for 2 min., In a second flask, proligand (1.0 eq.) was first dissolved in 10 mL dried acetonitrile slowly poured in first flask with the simultaneous addition of sodium acetate (3.0 eq.). The solution was allowed to be refluxed for 3–4 h that resulted in the formation of precipitates that were filtered, washed with ethanol and ether.

2.3.1. [Pd(L^1)(CH$_3$CN)]
Quantities: H$_2$L^1 (0.50 g, 1.6 mmol, 1.0 eq.), bis(benzonitrile)palladium dichloride (0.63 g, 1.6 mmol, 1.0 eq.), NaOAc (0.40 g, 4.8 mmol, 3.0 eq.), Reflux time: 3hrs.

Yield: 54 %, Color: light orange, M.p: 245–247 °C. FTIR: (KBr, cm^{-1}): 3032 (s), 2952 (s), 2854 (m), 1765 (m), 1618(m), 1554 (m), 1380 (m), 501 (s). ^{1}HNMR (300 MHz, (CD$_3$)$_2$SO, δ ppm): δ 10.65 (s, 1H, —CH), 8.25 (d, $J = 6$ Hz, 1H, Ar-H), 7.98 (d, $J = 3.3$ Hz, 1H, Ar-H), 7.75 (d, $J =$

3.9 Hz, 1H, Ar-H), 7.34 (t, $J = 3.6$ Hz, 2H, Ar-H), 7.20 (t, $J = 3.6$ Hz, 1H, Ar-H), 6.89 (t, $J = 4.2$ Hz, 2H, Ar-H), 6.79 (m, 2H, Ar-H), 6.61 (d, $J = 6$ Hz, 1H, Ar-H), 6.60 (m, 1H, Ar-H), 4.74 (s, 2H, CH$_2$), 1.71 (s, 3H, CH$_3$). ^{13}CNMR (75 MHz, (CD$_3$)$_2$SO, δ ppm): 165.8, 159.8, 154.4, 150.7, 144.2, 140.1, 135.4, 133.2, 130.1, 129.9, 128.7, 126.8, 125.1, 122.7, 120.7, 119.6, 117.7, 44.3, 28.7. Elem. Anal. for C$_{21}$H$_{18}$N$_4$OPd: C, 56.20; H, 4.04; N, 12.48; Found: C, 56.69; H, 3.58; N, 12.09.

2.3.2. [Pd(L^2)(CH$_3$CN)]

Quantities: H$_2$L^2 (0.40 g, 1.0 mmol, 1.0 eq.), bis(benzonitrile)palladium dichloride (0.40 g, 1.0 mmol, 1.0 eq.), NaOAc (0.32 g, 3.0 mmol, 3.0 eq.), Reflux time: 3hrs.

Yield: 59 %, Color: light orange, M.p: 264–266 °C. FTIR: (KBr, cm^{-1}): 3065 (m), 29,642 (m), 2932 (m), 2831 (m), 1765 (m), 1675 (s), 1543 (m), 1364 (m), 519 (s). ^{1}H NMR (300 MHz, (CD$_3$)$_2$SO, δ ppm): 9.54 (s, 1H, CH), 8.52 (d, $J = 3$ Hz, 1H, Ar-H), 8.17 (d, $J = 6$ Hz, 1H, Ar-H), 7.60 (d, $J = 3.6$ Hz, 1H, Ar-H), 7.40 (t, $J = 3.9$ Hz, 3H, Ar-H), 7.35 (d, $J = 3.9$ Hz, 2H, Ar-H), 7.21 (d, $J = 6.6$ Hz, 1H, Ar-H), 6.89 (d, $J = 3.3$ Hz, 1H, Ar-H), 6.68 (m, 1H, Ar-H), 4.38 (s,1H,—CH$_2$), 1.65 (s, 3H, CH$_3$). ^{13}C NMR (75 MHz, (CD$_3$)$_2$SO, δ ppm): 166.1, 155.3, 151.2, 149.8, 148.9, 145.5, 142.1, 139.5, 135.4, 130.6, 129.7, 127.9, 124.5, 121.4, 120.7,118.5, 115.8, 44.3, 25.9. Elem. Anal. for C$_{21}$H$_{17}$BrN$_4$OPd: C, 47.80; H, 3.25; N, 10.62; Found: C, 47.35; H, 3.01; N, 10.16.

2.3.3. [Pd(L^3)(CH$_3$CN)]

Quantities: H$_2$L^3 (0.40 g, 1.1 mmol, 1.0 eq.), Bis(benzonitrile)palladium dichloride (0.43 g, 1.1 mmol, 1.0 eq.), NaOAc (0.27 g, 3.3 mmol, 3.0 eq.), Reflux time: 4hrs.

Yield: 63 %, Color: Yellow, M.p: 241–243 °C. FTIR: (KBr, cm^{-1}): 3057 (s), 2997 (s), 2920 (m), 2850 (m), 2354 (m), 2335 (m), 1723 (m), 1615 (m), 1358 (m), 505 (s). ^{1}HNMR (300 MHz, (CD$_3$)$_2$SO, δ ppm): 9.56 (s, 1H, —CH), 8.70 (d, $J = 2.1$ Hz, 1H, Ar-H), 8.59 (d, $J = 3.9$ Hz, 1H, Ar-H), 7.87 (d, $J = 4.5$ Hz, 1H, Ar-H), 7.80 (d, $J = 3.9$ Hz, 1H, Ar-H), 7.57 (t, $J = 4.2$ Hz, 1H, Ar-H), 7.48 (d, $J = 3.3$ Hz, 2H, Ar-H) 7.39 (d, $J = 3.6$ Hz, 5H, Ar-H), 7.10 (d, 1H, Ar-H), 4.78(s, 1H, CH$_2$), 1.54 (s,3H,CH$_3$). ^{13}CNMR (75 MHz, (CD$_3$)$_2$SO, δ ppm): 161.1, 159.7, 152.8, 146.6, 145.2, 141.0, 136.7135.6, 134.6, 130.6, 129.2, 128.1, 128.9, 127.3, 126.4, 124.7, 121.4, 119.7, 118.9, 112.4, 110.1, 47.1, 19.8. Elem. Anal. for C$_{21}$H$_{17}$BrN$_4$OPd: C, 60.19; H, 4.04; N, 11.23; Found: C, 60.43; H, 3.65; N, 11.61.

2.3.4. [Pd(L^4)(CH$_3$CN)]

Quantities: H$_2$L^4 (0.30 g, 0.8 mmol, 1.0 eq.), Bis(benzonitrile)palladium dichloride (0.30 g, 0.8 mmol, 1.0 eq.), NaOAc (0.19 g, 2.4 mmol, 3.0 eq.), Reflux time: 4hrs.

Yield: 67 %, Color: Yellow, M.p: 276–278 °C. FTIR: (KBr, cm^{-1}): 3149 (m), 2962 (m), 2928 (m), 2857 (m), 1731(m), 1604 (s), 1589 (m), 1373 (m), 504 (s). ^{1}HNMR (300 MHz, (CD$_3$)$_2$SO, δ ppm): 8.20 (s, 1H, —CH), 7.88 (m, 1H, Ar-H), 7.44 (d, $J = 7.2$ Hz, 1H, Ar-H), 7.14 (m, 2H, Ar-H), 7.04 (m, 3H, Ar-H), 6.60 (m, 2H, Ar-H), 6.43 (d, $J = 2.4$ Hz, 2H, Ar-H), 4.32 (s, 2H, —CH$_2$), 3.39 (q, $J = 6.9$ Hz, 4H, —CH$_2$), 1.75 (s,3H, CH$_3$), 1.13 (d, $J = 6.9$ Hz, 6H, —CH$_3$). ^{13}CNMR (75 MHz, (CD$_3$)$_2$SO, δ ppm): 165.1, 163.0, 160.9, 157.0, 155.5, 152.8, 149.2, 145.9, 140.7, 137.4, 132.7, 129.5, 124.7, 121.6, 120.7, 118.2, 110.8, 45.2, 44.6, 24.6, 12.8. Elem. Anal. for C$_{25}$H$_{27}$N$_5$OPd: C, 57.75; H, 5.23; N, 13.47; Found: C, 58.20; H, 5.67; N, 13.05.

2.3.5. [Pd(L^5)(CH$_3$CN)]

Quantities: H$_2$L^5 (0.40 g, 1.0 mmol, 1.0 eq.), Bis(benzonitrile)palladium dichloride (0.41 g, 1.0 mmol, 1.0 eq.), NaOAc (0.26 g, 3.1 mmol, 3.0 eq.), Reflux time: 3hrs.

Yield: 54 %, Color: light orange, M.p: 233–235 °C· FTIR: (KBr, cm^{-1}): 2925 (m), 2852 (m), 2359 (m), 2341 (m), 1716 (m), 1643 (m), 1597 (m), 1372 (m), 507 (s). ^{1}HNMR (300 MHz, (CD$_3$)$_2$SO, δ ppm): 9.35 (s, 1H, —CH), 8.85 (d, $J = 3.9$ Hz, 1H, Ar-H), 8.47 (d, $J = 3.3$ Hz, 1H, Ar-H), 8.10 (d, $J = 3.9$ Hz, 1H, Ar-H), 7.93 (d, $J = 6$ Hz, 1H, Ar-H) 7.36 (d, $J =$

3.6 Hz, 1H, Ar-H), 7.24 (m, 1H, Ar-H), 3.92 (m, 1H, Cy-H), 1.91 (s, 3H, CH$_3$), 1.76 (m, 3H, Cy-H), 1.57 (m, 4H, Cy-H), 1.28 (m, 2H, Cy-H). ^{13}CNMR (75 MHz, (CD$_3$)$_2$SO, δ ppm): 164.7, 162.7, 157.8, 155.9, 149.5, 145.8, 142.2, 138.9, 135.4, 130.7, 125.4, 121.9, 120.2, 49.2, 32.9, 25.7, 25.0, 21.5. Elem. Anal. for C$_{20}$H$_{21}$BrN$_4$OPd: C, 46.22; H, 4.07; N, 10.78; Found: C, 46.65; H, 4.49; N, 10.39.

2.3.6. [Pd(L^6)(CH$_3$CN)]

Quantities: H$_2$L^6 (0.30 g, 0.8 mmol, 1.0 eq.), Bis(benzonitrile)palladium dichloride (0.31 g, 0.8 mmol, 1.0 eq.), NaOAc (0.20 g, 2.4 mmol, 3.0 eq.), Reflux time: 4hrs.

Yield: 59 %, Color: light yellow, M.p: 253–255 °C· FTIR: (KBr, cm^{-1}): 2925 (m), 2847 (m), 2398 (m), 2343 (m),1731 (m), 1652 (m), 1586 (m), 1368 (m), 510 (s). ^{1}HNMR (300 MHz, (CD$_3$)$_2$SO, δ ppm): 8.41 (s, 1H, CH), 7.81 (d, $J = 6.3$ Hz, 1H, Ar-H), 7.32 (d, $J = 6.5$ Hz, 1H, Ar-H), 7.25 (d, $J = 3.6$ Hz, 2H, Ar-H), 6.98 (m, 1H, Ar-H), 6.27 (m, 1H, Ar-H), 3.96 (m, 1H, Cy-H), 3.49 (q, $J = 3.9$ Hz, 4H, —CH$_2$), 1.60 (m, 4H, Cy-H), 1.42 (m, 2H, Cy-H), 1.39 (m, 4H, Cy-H), 1.79 (s, 3H, —CH$_3$), 1.29 (t, $J = 6.3$ Hz, 6H, —CH$_3$). ^{13}CNMR (75 MHz, (CD$_3$)$_2$SO, δ ppm): 164.9, 162.8, 159.4, 155.6, 153.7, 150.2, 149.4, 141.7, 134.3, 125.8, 120.5, 117.3, 110.9, 48.8, 48.7, 44.2, 25.7, 24.9, 22.3, 12.0. Elem. Anal. for C$_{24}$H$_{31}$N$_5$OPd: C, 56.31; H, 6.10; N, 13.68; Found: C, 56.01; H, 6.47; N, 13.99.

2.3.7. [Pd(L^7)(CH$_3$CN)]

Quantities: H$_2$L^7 (0.50 g, 1.3 mmol, 1.0 eq.), Bis(benzonitrile)palladium dichloride (0.50 g, 1.3 mmol, 1.0 eq.), NaOAc (0.31 g, 3.9 mmol, 3.0 eq.), Reflux time: 4 h.

Yield: 65 %, Color: light yellow, M.p: 242–244 °C. FTIR: (KBr, cm^{-1}): 3043 (s), 2922 (m), 2852 (m), 1737 (m), 1616 (m), 1570 (m), 1290 (m), 498(s). ^{1}HNMR (300 MHz, (CD$_3$)$_2$SO, δ ppm): 8.98 (s, 1H, CH), 8.36 (d, $J = 6$ Hz, 1H, Ar-H), 8.12 (m, 1H, Ar-H), 7.61 (d, $J = 3.3$ Hz, 1H, Ar-H), 7.33 (d, $J = 6$ Hz 1H, Ar-H), 7.61 (m, 3H, Ar-H), 7.00 (d, $J = 3$ Hz, 2H, Ar-H), 6.94 (m, 1H, Ar-H), 2.36 (s, 3H, CH$_3$), 1.67 (s, 3H, CH$_3$). ^{13}CNMR (75 MHz, (CD$_3$)$_2$SO, δ ppm): 165.2, 161.7, 158.9, 157.2, 152.0, 148.9, 144.6, 140.4, 135.7, 131.2, 128.2, 123.4, 122.5, 122.1, 121.9, 120.4, 120.1, 117.3, 112.8, 43.2, 18.5. Elem. Anal. for C$_{21}$H$_{17}$BrN$_4$OPd: C, 47.80; H, 3.25; N, 10.62; Found: C, 47.39; H, 3.62; N, 10.29.

2.3.8. [Pd(L^8)(CH$_3$CN)]

Quantities: H$_2$L^8 (0.40 g, 1.0 mmol, 1.0 eq.), Bis(benzonitrile)palladium dichloride (0.41 g, 1.0 mmol, 1.0 eq.), NaOAc (0.26 g, 3.1 mmol, 3.0 eq.), Reflux time: 4hrs.

Yield: 52 %, yellow, M.p: 241–243 °C. FTIR: (KBr, cm^{-1}): 3128 (m), 3012 (m), 2958 (m), 2876 (m),1761 (m), 1654 (m), 1544 (m), 1292 (m), 479 (s). ^{1}HNMR (300 MHz, (CD$_3$)$_2$SO, δ ppm): 8.50 (s, 1H, —CH), 8.06 (d, $J = 6$ Hz, 2H, Ar-H), 7.49 (d, $J = 7$ Hz, 1H, Ar-H), 7.38 (d, $J = 3.6$ Hz, 1H, Ar-H), 7.22 (m, 1H, Ar-H), 7.22 (d, $J = 6$ Hz, 2H, Ar-H), 6.76 (m, 1H, Ar-H), 6.50 (d, $J = 3.3$ Hz, 2H, Ar-H), 3.32 (q, $J = 6$ Hz, 4H, —CH$_2$), 2.41 (s, 3H, —CH$_3$), 2.27 (d, $J = 6.9$ Hz, 6H, —CH$_3$), 1.63 (s, 3H, —CH$_3$). ^{13}C NMR (75 MHz, (CD$_3$)$_2$SO, δ ppm): 166.5, 163.2, 161.4, 158.9, 155,3, 151.7, 147.3, 144.6, 140.1, 137.6, 134.2, 130.8, 129.4, 127.7, 124.6, 122.5, 121.2, 120.7, 119.2, 46.4, 43.6, 18.7, 12. 7. Elem. Anal. for C$_{25}$H$_{27}$N$_5$OPd: C, 57.75; H, 5.23; N, 13.47; Found: C, 57.32; H, 5.59; N, 13.10.

2.4. In vitro cytotoxicity assay of metal complexes

In Vitro cytotoxicity assay of metal complexes was determined by performing an MTT (yellow tetrazolium salt, 3-(4, 5-dimethylthizol-2-yl)-2, 5- diphenyl tetrazolium bromide) assay by using an aggressive Breast cancer cell lines MDA-MB (ATCC) and MCF-7. These cell lines are ER, PR, and E-cadherin negative and expresses mutated p53 since the MDA-MB-231 lack the growth factor receptor HER2, they represent a good model of triple-negative breast cancer and is commonly used for In-vitro and In-vivo study (Welsh, 2013). Human breast Normal cell line

MCF-10A (Iranian biological resource Centre IBRC Tehran, Iran) were keep as a control in the study. Cells were cultured in DMEM supplemented with 10 % FBS and 1 % antibiotics (100 U/ml penicillin). The cells were seeded in a 96-well plate at a density of 1.0×10^4 cells/well and incubated for 24 h at 37 °C in 5 % CO_2. The medium was discarded, and both the cell lines were treated with different concentration (5 μM, 10 μM, 25 μM, and 50 μM) of metal complexes (Maher et al., 2019). After 48 h of incubation, 20 μL of MTT solution (5 mg/mL) was pipetted into each well and incubated for another 4 h (Sakhi et al., 2022). The medium was later discarded, and the formazan precipitate was dissolved in DMSO. The absorbance of the mixtures was determined using a micro-plate reader at 570 nm. All experiments were performed in triplicates and cytotoxicity was expressed as percentage of cell viability compared to untreated control cells (Maher et al., 2019).

$$\%Viability = \frac{Absorbance\,of\,sample}{Absorbance\,of\,control} \times 100 \#$$

2.5. Solution studies

Three representative compounds $[Pd(L^1)(CH_3CN)\text{-} \quad [Pd(L^3)(CH_3CN)]$ were analyzed by UV–Vis spectroscopy for their stability in solutions. Small amounts of respective compounds were first dissolved in DMSO and then the solutions were diluted by addition of small quantity DI water. The concentration of complexes in the final solutions were equal to 5×10^{-5} M. The resulted solutions were then subjected to UV–Vis absorption at different time interval (0 min, 1 h, 2 h, 3 h and 24 h) at room temperature.

2.6. Molecular docking

2.6.1. Structure optimization

The optimization of palladium complexes was conducted using the Gaussian 09 software package. The optimization was performed with the B3LYP density functional. The basis set employed for H, C, O, atoms was the 6-31G(d) basis set, including only the five spherical harmonic components of the polarization functions (Sumrra et al., 2022a, 2022b). For Pd, we used the corresponding Stuttgart relativistic Effective Core Potentials (ECPs) to represent the core electrons, numbering 28, 28, and 46 electrons, respectively. These were paired with their associated triple zeta basis as implemented in Gaussian. Additional polarization functions were added, including an f function for Pd (exponent 1.14844). This combination of basis sets is referred to as BS1. Frequencies were calculated using the B3LYP/BS1 level of theory. These calculations were essential for characterizing stationary points, determining zero-point energies, and deriving gas-phase statistical mechanics values for thermal and entropic corrections at specified temperatures.

2.6.2. Preparation of complexes using ligprep from Schrodinger

The chemical structures of all complexes were drawn using the 2D sketcher tool in Schrodinger. Subsequently, the structures were subjected to preparation and optimization using the LigPrep module. During this process, energy minimization and correction of 3D geometry were performed. The ionization states of the ligands remained unchanged. The output files generated by LigPrep were utilized directly for docking simulations and the calculation of Absorption, Distribution, Metabolism, and Excretion (ADME) properties. Screening of ADME properties was accomplished using the QuikProp module.

2.6.3. Protein preparation and receptor grid generation

The protein structure, obtained from the Protein Data Bank for tyrosine kinases namely EGFR, VEGFR, FGFR, HGFR and SRC, was utilized as the starting point for protein preparation. The Protein preparation Wizard was employed to perform the following tasks: addition of missing chain residues, inclusion of hydrogen bonds, and removal of water molecules. Subsequently, energy minimization was performed to optimize the protein structure. The resulting output file was used to generate the receptor grid. The grid was generated to encompass the ligand-binding site in the protein, defining the docking site. The size of the grid was set to match the workspace of the ligand, with a default size of 20 Å. The output of the glide grid file was used for docking simulations.

2.6.4. Complexes docking with extra precision mode (XP)

The Glide grid file generated in the previous step and the LigPrep file were employed as input for Pd(II) complexes docking simulations. The docking was performed using the extra precision mode (XP) of the Glide docking algorithm, which allows for flexible docking of complex. At the completion of the docking process, docking scores, hydrogen bond interactions, hydrophobic interactions, and other relevant details were recorded and analyzed for each compound. This methodology ensured the proper preparation of ligands and the protein receptor, enabling the accurate docking of complex in the active site of the target protein. The use of extra precision docking mode (XP) facilitated the exploration of ligand flexibility, leading to a comprehensive assessment of ligand-protein interactions and potential binding affinities.

2.7. Cell apoptosis induction assay

Cell apoptosis induced by the tested compounds was assessed using the Dead Cell Apoptosis Kit, employing Annexin V FITC and propidium iodide (PI) staining for subsequent flow cytometric analysis. Breast cancer cells were cultured, treated with synthesized compounds, and harvested. After washing, cells were stained with Annexin V FITC and PI as per the kit protocol. Flow cytometric analysis was then conducted to determine cell populations: live, early apoptotic (Annexin V FITC positive, PI negative), late apoptotic/necrotic (double-positive for Annexin V FITC and PI), and viable (negative for both stains). This methodology enabled quantification of apoptotic induction and identification of viable cell populations, contributing to a comprehensive understanding of the tested compounds' apoptotic impact.

3. Results

3.1. Chemistry

a) Proligands

Synthesis of proligands were synthesized in three steps as shown in Scheme 1. In the first step, 2-chloro-3-nitropyridine was treated individually with benzyl amine, cyclohexyl amine and o-toluidine to form nitro containing compounds (1–3). The nitro group was then catalytically reduced to primary amine using 10 % activated palladium on charcoal and hydrazine hydrated in ethanol to form precursors (4–6). In the third and final step 4–6 were reacted separately with four different aldehydes namely 2-hydroxybenzaldehyde, 5-bromo-2-hydroxybenzaldehyde, 2-hydroxy-1-naphthaldehyde and 4-(diethylamino)-2-hydroxybenzaldehyde) to form respective proligands (H_2L^1-H_2L^8). All the precursors (1–6) and proligands (H_2L^1-H_2L^8) were purified by column chromatography and characterized by FTIR, ^{1}HNMR, ^{13}CNMR and single crystal XRD analysis.

The compound N^2-benzylpyridine-2, 3-diamine (4) was crystalized in acetone by slow evaporation at room temperature and brown colored fine crystals were obtained. The ORTEP diagram (shown in Fig. 2) clearly indicated the successful reduction of nitro group into primary amine. Based on the data collected, the structure in which the precursor (4) was crystalized is monoclinic with the space group P 2_1 /n, with Z = 4 (Fig. 3) for the formula unit, $C_{12}H_{13}N_3$. The other crystallographic parameters shows that empirical formula of the compound is $C_{11}H_{17}N_3$. The final cell constants of a = 10.960(3) Å, b = 9.1095(19) Å, c = 11.861 (3) Å, α = 90°, β = 116.087(6), γ = 90°, volume = 1063.57 Å^3.
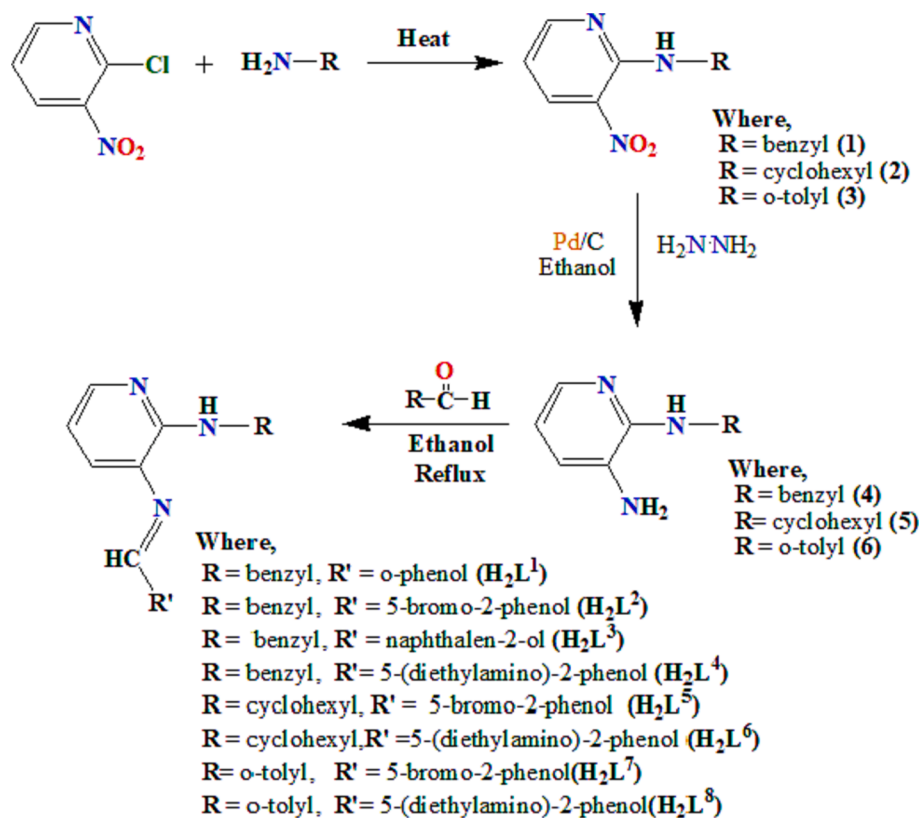
Scheme 1. Synthesis of proligands (H_2L^1) – (H_2L^8).
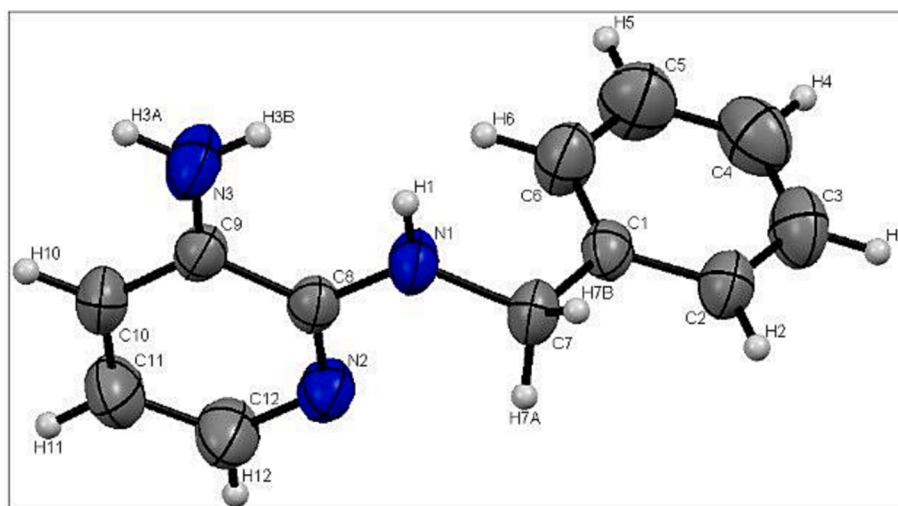
Fig. 2. ORTEP diagram of N^2-benzylpyridine-2,3-diamine **(4)**.

b) Pd(II) complexes [Pd(L^1)(CH$_3$CN)] – [Pd(L^8)(CH$_3$CN)]

Palladium(II) complexes were synthesized by reacting bis(benzonitrile)palladium dichloride with proligands **(H_2L^1-H_2L^8)** in 1:1 in the presence of sodium acetate a base for abstraction of proton from both –OH group and –NH moieties of proligand during complex formation reaction (Scheme 2). This resulted in the generation of NNO tridentate proligands. All the palladium complexes were purified by recrystallization and characterized by FTIR, ^{1}HNMR and ^{13}CNMR and computational studies.

3.2. Structure optimization

The optimized structure for **[Pd(L^1)CH$_3$CN)]** was calculated by using Gauss View method. The optimized square planner geometry (optimum frequency) of palladium complex and bond lengths shown in Fig. 4. Vibrational analyses were conducted using the B3LYP/BS1 level of theory. These frequency calculations served several crucial purposes, including the characterization of stationary points, the determination of zero-point energies, and the derivation of gas-phase statistical mechanics data pertaining to thermal and entropic corrections, as required for the specified temperatures. In these statistical mechanics calculations, we employed the simplified rigid-rotor harmonic oscillator
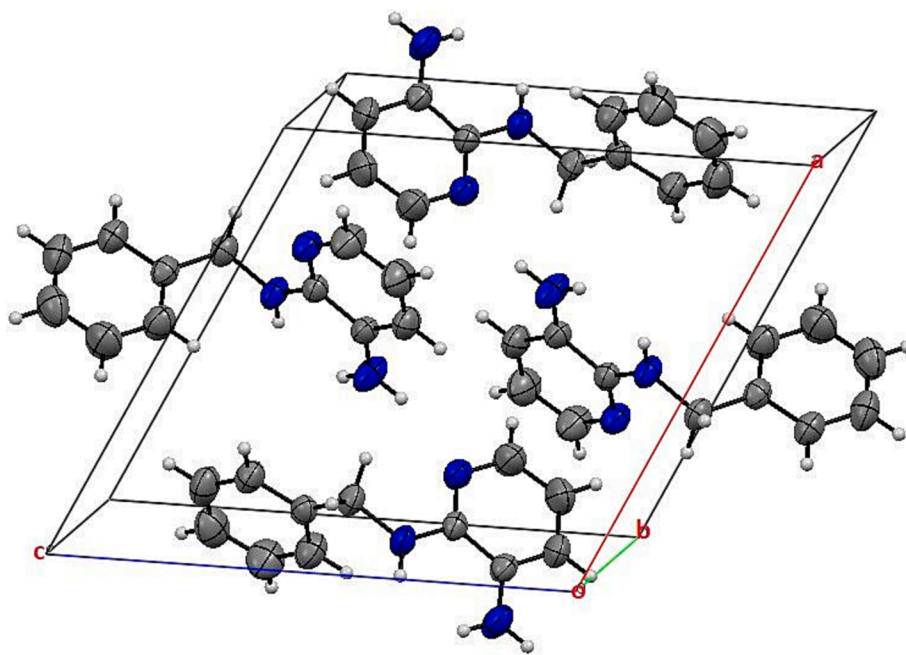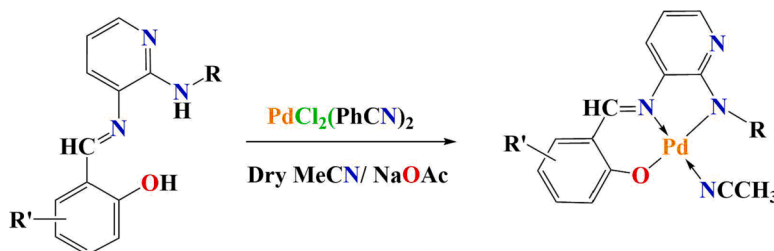
Fig. 3. Unit cell representation of N^2-benzylpyridine-2,3-diamine **(4)**.

Where,

R = benzyl, R' = H	**[Pd(L^1)(CH$_3$CN)]**
R = benzyl, R' = 5-Br	**[Pd(L^2)CH$_3$CN)]**
R = benzyl, R' = C$_4$H$_4$	**[Pd(L^3)(CH$_3$CN)]**
R = benzyl, R' = 4-N(Et)$_2$	**[Pd(L^4)(CH$_3$CN)]**
R = cyclohexyl, R' = 5-Br	**[Pd(L^5)(CH$_3$CN)]**
R = cyclohexyl, R' = 4-N(Et)$_2$	**[Pd(L^6)(CH$_3$CN)]**
R = o-tolyl, R' = 5-Br	**[Pd(L^7)(CH$_3$CN)]**
R = o-tolyl, R' = 4-N(Et)$_2$	**[Pd(L^8)(CH$_3$CN)]**

Scheme 2. Synthesis of complexes **[Pd(L^1)(CH$_3$CN)] – [Pd(L^8)(CH$_3$CN)]** .

approximation. It is worth noting that the accuracy of computed entropies is highly sensitive to potential numerical errors in the values of the lowest-frequency modes. To mitigate this, we conducted a thorough visual inspection of these modes for all species. Among the observed vibrational modes, soft torsional modes with frequencies below 1500 cm^{-1} were common, with values lower than 7 cm^{-1} being a rarity shown in **Fig. S26.** In vibrational analysis, no imaginary frequency value is observed that confirm the stationary points (Noreen and Sumrra, 2022). The location of frontier orbitals, their energy values and resultant band gap is shown in Fig. 5. It is clear that the electron density is spread over the aromatic rings and heteroatoms and metallic part of complex.

3.3. Chemical reactivity Parameters

In addition to the reactive site peculiarities of chemical systems, DFT is useful for quantifying a variety of global reactivity descriptors that are used to assess chemical reactivity. Frontier molecular orbital is an excellent tool for examining and characterizing chemical reactivity properties, such as the analyzed molecules' capacity to absorb and donate as well as their hardness and softness (Seghir et al., 2019). Chemically hard molecules in nature are those having a high FMO energy difference because they are more stable and kinetically least reactive. On the other hand, molecules with narrow FMO band gaps are more polarizable, less stable, and chemically soft due to their higher kinetic reactivity. The FMO energy gap can also be used to derive global reactivity parameters(Simović et al., 2019, Sumrra et al., 2021), such as ionization potential (IP), electron affinity (EA), global hardness (η), global softness (σ), chemical potential (μ), global electrophilicity (ω), and electronegativity (χ) by using Eqs. (1)–(5) (Arjunan et al., 2009, Madhavan et al., 2009, Obi-Egbedi et al., 2011, Karabacak et al., 2014) and the values of global reactivity descriptors are given in Table 1 (58–61)
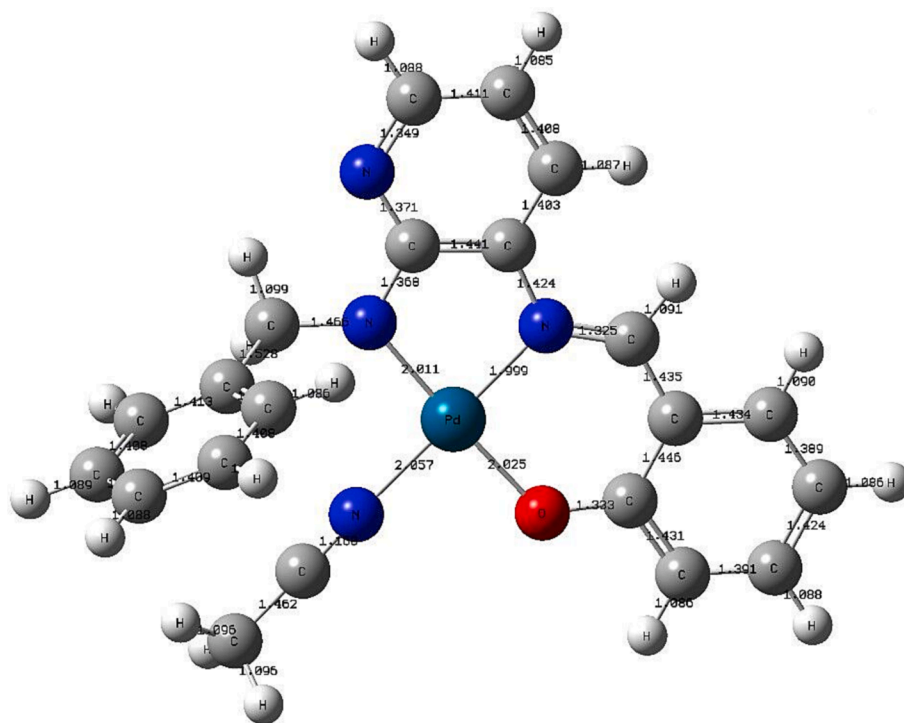
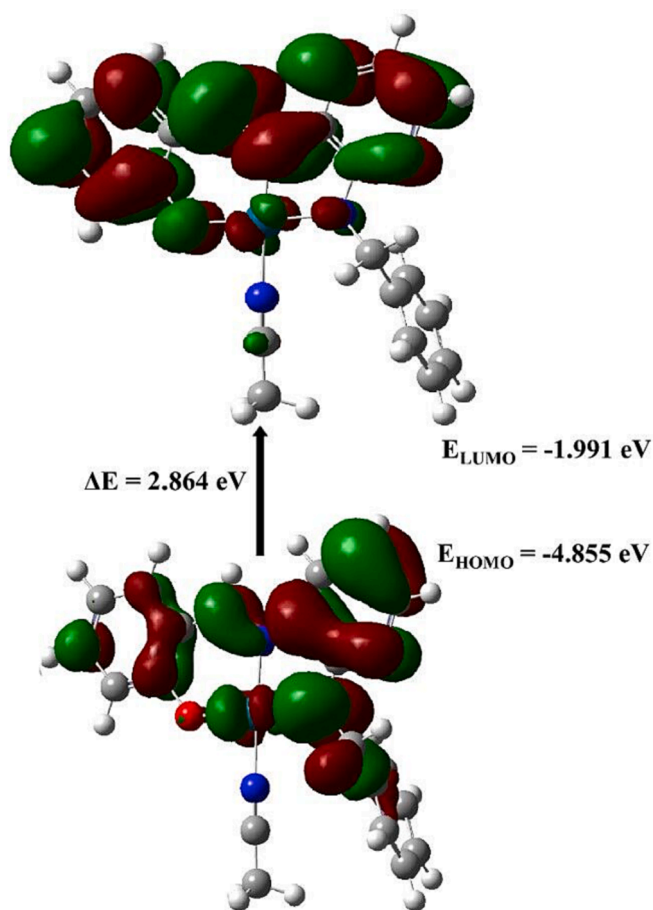**Fig. 4.** The optimized structure of complex [Pd(L^1)CH$_3$CN].

Fig. 5. Energy levels of the HOMO and LUMO for complex [Pd(L^1)CH$_3$CN].

$$IP = -E_{(HOMO)}$$

$$EA - E_{(HOMO)} \tag{1}$$

$$\mu = \frac{E_{(HOMO)} + E_{(LUMO)}}{2}$$

$$x = \frac{[IP + EA]}{2} = -\left[\frac{E_{(LUMO)} + E_{(HOMO)}}{2}\right] \tag{2}$$

$$\eta = \frac{[IP - EA]}{2} = -\left[\frac{E_{(LUMO)} - E_{(HOMO)}}{2}\right] \tag{3}$$

$$\sigma = 1/2\,\eta \tag{4}$$

$$\omega = \mu^2/2\eta \tag{5}$$

3.4. Cytotoxicity evaluation against breast cell lines

Various concentrations (5 μM, 10 μM, 25 μM, and 50 μM) of precursor (**1–6**), pro-ligand (**H$_2$L^1 – H$_2$L^8**) and palladium complexes, **[Pd(L^1)(CH$_3$CN)] – [Pd(L^8)(CH$_3$CN)]** were used to find out their growth inhibition potential against the human breast cancer cell lines namely MDA-MB-231 and MCF-7. At the same time human normal breast epithelial cell lines, MCF-10A were kept as a control in the experiment. The MTT [3-(4, 5-dimethylthiazol-2-yl)-2, 5-diphenyltetrazolium bromide] assay was used to determine the decrease in cancer cell viability induced by cytotoxic agents. For MDA-MB-231, MCF-7 and MCF-10A the IC$_{50}$ values of all the compounds are presented in Table 2. IBM SPSS Statistics 26 software was utilized to analyze the dose–response and computation IC$_{50}$ values.

3.5. Cell apoptosis

In our pursuit to understand the apoptotic induction mechanism of the synthesized complexes within breast cancer cells, an array of resultant compounds was meticulously assessed as shown in Fig. 7.
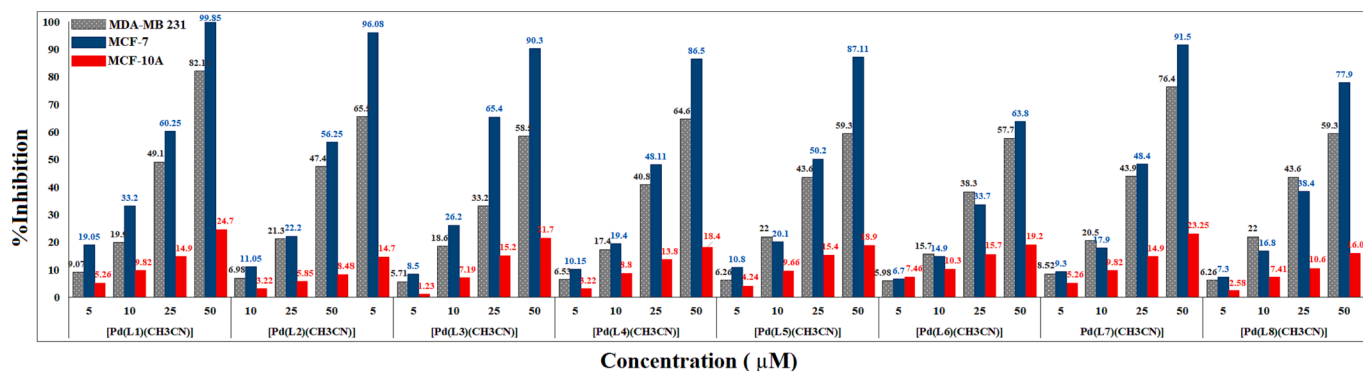
Fig. 6. Percent inhibition of metal complexes on Breast cancer cell lines (MDA-MB-231 and MCF-7) and on normal breast cell line (MCF-10A).

Table 1
Chemical reactivity parameter for [Pd(L^1)CH$_3$CN)].

Electron affinity	0.073
Ionization potential	0.178
Electronegativity	0.125
Global hardness	0.052
Global softness	9.501
Global electrophilicity	0.150
Chemical potential	−0.125

Table 2
IC$_{50}$ values (±SD) of precursors, proligands, complexes and cisplatin.

ID	IC$_{50}$ Values (μM)		
	MDA-MB-231	MCF-7	MCF-10A
1	110.01 ± 0.40	122.01 ± 0.80	>100
2	110.20 ± 0.30	118.02 ± 0.30	>100
3	112.02 ± 0.41	120.01 ± 0.30	>100
4	108.01 ± 0.20	109.03 ± 0.60	>100
5	109.02 ± 0.80	112.01 ± 0.41	>100
6	108.02 ± 0.20	112.01 ± 0.20	>100
H$_2$L^1	75.01 ± 0.20	70.90 ± 0.40	>100
H$_2$L^2	81.60 ± 0.60	70.50 ± 0.41	>100
H$_2$L^3	87.01 ± 0.30	112.40 ± 0.60	>100
H$_2$L^4	81.10 ± 0.20	104.61 ± 0.20	>100
H$_2$L^5	82.20 ± 0.60	88.81 ± 0.81	>100
H$_2$L^6	96.00 ± 0.40	99.60 ± 0.41	>100
H$_2$L^7	85.10 ± 0.40	88.30 ± 0.51	>100
H$_2$L^8	83.60 ± 0.30	88.30 ± 0.30	>100
[Pd(L^1)(CH$_3$CN)]	**25.50 ± 0.30**	**20.76 ± 0.30**	>100
[Pd(L^2)(CH$_3$CN)]	27.51 ± 0.30	24.40 ± 0.20	>100
[Pd(L^3)(CH$_3$CN)]	41.30 ± 0.40	38.00 ± 0.40	>100
[Pd(L^4)(CH$_3$CN)]	34.40 ± 0.20	27.70 ± 0.30	>100
[Pd(L^5)(CH$_3$CN)]	34.20 ± 0.20	27.10 ± 0.20	>100
[Pd(L^6)(CH$_3$CN)]	40.60 ± 0.30	38.60 ± 0.40	>100
[Pd(L^7)(CH$_3$CN)]	29.81 ± 0.60	26.90 ± 0.50	>110
[Pd(L^8)(CH$_3$CN)]	34.60 ± 0.80	32.10 ± 0.21	>100
Cisplatin	**27.00 ± 0.80**	**24.10 ± 0.80**	**64.6 ± 0.5**

3.6. Stability of complexes [Pd(L^1)(CH$_3$CN)] – [Pd(L^3)(CH$_3$CN)] in aqueous solutions

The solutions of complexes in DMSO-water mixture were analyzed by using UV–Vis spectroscopy for their stability assessment. After dissolving the complexes in DMSO followed by mixing of DI water, the resulted solutions were immediately tested for UV–Vis absorption. The solutions were then incubated in dark and their spectra were obtained after 1 h, 2 h, 3 h and 24 h. The resultant spectra of complexes are shown in Fig. 8. The results show no change in absorption peaks and slight decrease in UV–Vis absorption of complexes after incubation for 24 h.

3.7. Computational assessment for tyrosine kinase Inhibitors

An extensive in silico evaluation of palladium complexes, **[Pd(L^1)(CH$_3$CN)] – [Pd(L^8)(CH$_3$CN)]**, were carried out to assess their potential as tyrosine kinase inhibitors mentioned in Table 3. In the first step, the structure of the complexes was optimized using default parameters in GuassView.

Our analysis incorporated absorption, distribution, metabolism, and excretion (ADME) properties and docking values against key tyrosine kinases (EGFR, VEGFR, FGFR, HGFR, and SRC) are shown in Table 4. The compounds were ranked based on their overall scores, calculated by assigning appropriate weights according to the previous studies, to each ADME property and docking score. The weighting scheme was as follows: absorption (30 %), distribution (25 %), metabolism (20 %), excretion (10 %), and docking Values (15 %).

4. Discussion

All the compounds were initially characterized by FTIR. The stretching band for NH (secondary amine) of **1–6** originated between 3396 and –3337 cm^{-1} and for proligands (H$_2$L^1-H$_2$L^8) appeared at 3592–3338 cm^{-1}. Precursors (**4–6**) showed bands for NH$_2$ moiety at 3233, 3060, 3330, 3131, 3340, 3226 cm^{-1} indicated the reduction of NO$_2$ group into primary amine group and were disappeared in the IR spectra of all the proligands. The new OH stretching band appeared between 3378 and 3199 cm^{-1} in all proligands indicated the successful synthesis of H$_2$L^1-H$_2$L^8. Similarly, the aromatic C—H stretch originated at 3112–2922 cm^{-1} and aliphatic C—H stretch appeared at 2876–2842 cm^{-1}. In FTIR spectra of complexes **[Pd(L^1)(CH$_3$CN)] – [Pd(L^8)(CH$_3$CN)]**, the band for NH and OH groups were disappeared in all Pd (II) complexes, a new ν(Pd-N) band appeared at 479–510 cm^{-1} within the acceptable range (438–528 cm^{-1}) of Pd-N linkage (Durig et al., 1965).

In ^{1}HNMR spectra, NH proton originated as triplet peak in **1, 4** at 8.97, 6.04 ppm and as doublet peak in **2, 5** at 8.14, 5.21 ppm and singlet peak of one proton at 9.86, 6.00 ppm for **3, 6**. A new characteristic peak of two protons of NH$_2$ group originated at 4.67, 4.68 and 3.47 ppm in **4–6** suggested the successful reduction of NO$_2$ group to NH$_2$ moiety. The disappearance of peak for NH$_2$ group and appearance of new singlet peak for azomethine moiety between 10.92 and 8.53 ppm as well as singlet peak for hydroxyl moiety at 14.68–11.98 ppm confirmed the formation proligands (H$_2$L^1-H$_2$L^8). The NH signal appeared in proligands as a triplet (6.84–6.13 ppm), doublet (5.47, 5.23 ppm) and singlet (7.36, 7.02 ppm) depending upon adjacent group (benzyl, cyclohexyl or tolyl groups respectively). The peaks associated with protons of aromatic ring and pyridine ring appeared at their respective positions. All the resulted Pd(II) complexes showed the disappearance of singlet peak of hydroxyl group and triplet/doublet/singlet peak of NH proton and the appearance of new singlet peak of three protons for methyl group of acetonitrile in the range of 1.79–1.54 ppm. In ^{13}CNMR of proliands, the

Table 3
In Silico evaluation of [Pd(L¹)(CH₃CN)] – [Pd(L⁸)(CH₃CN)] and their potential as tyrosine kinase inhibitors.

ID	S	MW	HBd	HBa	QPlogP o/w	QP logS	QP PCaco	PHOA	RO5
[Pd(L¹)(CH₃CN)]	1	456.89	1	8.0	3.786	3.98	567.34	95.3	1
[Pd(L²)(CH₃CN)]	1	399.19	2	7.1	4.000	4.89	700.45	99.0	0
[Pd(L³)(CH₃CN)]	0	600.34	2	6.0	5.245	4.61	589.11	95.8	0
[Pd(L⁴)(CH₃CN)]	0	566.45	2	6.0	5.128	5.01	767.00	99.0	0
[Pd(L⁵)(CH₃CN)]	0	411.89	2	6.6	3.122	−3.87	578.00	96.5	1
[Pd(L⁶)(CH₃CN)]	0	589.00	1	7.0	3.880	−5.12	734.00	95.7	0
[Pd(L⁷)(CH₃CN)]	1	527.72	2	6.6	3.883	−5.12	648.56	98.0	0
[Pd(L⁸)(CH₃CN)]	1	519.94	2	6.7	4.645	−5.34	736.00	98.4	0

Hbd and Hba: affinity of hydrogen bond donor and acceptor, **S (STARS):** S (STARS) represents the count of property or descriptor values that fall outside the 95% range of similar values observed in known drugs. The recommended range for S (STARS) is typically kept between 0 and 5, indicating the extent to which a compound's properties deviate from the norm observed in known drugs, **QPlogS:** QPlogS predicts the aqueous solubility of a compound and is expressed as the logarithm of its solubility value. The recommended range for QPlogS typically spans from −6.5 to −0.5, with more negative values indicating lower solubility and less negative values indicating higher solubility, **QPPCaco:** QPPCaco predicts the apparent permeability of a compound across Caco-2 cells, which serves as a model for intestinal absorption. The recommended range for QPPCaco suggests that values below 25 indicate poor permeability, while values above 500 indicate excellent permeability, **PHOA:** PHOA predicts the human oral absorption of a compound on a scale ranging from 0 to 100%. The recommended range for PHOA suggests that values exceeding 80% indicate high oral absorption, while values below 25% suggest poor oral absorption, **Ro5:** stands for Rule of 5, which is a set of guidelines used in drug discovery and development to assess the likelihood of a compound's oral bioavailability.
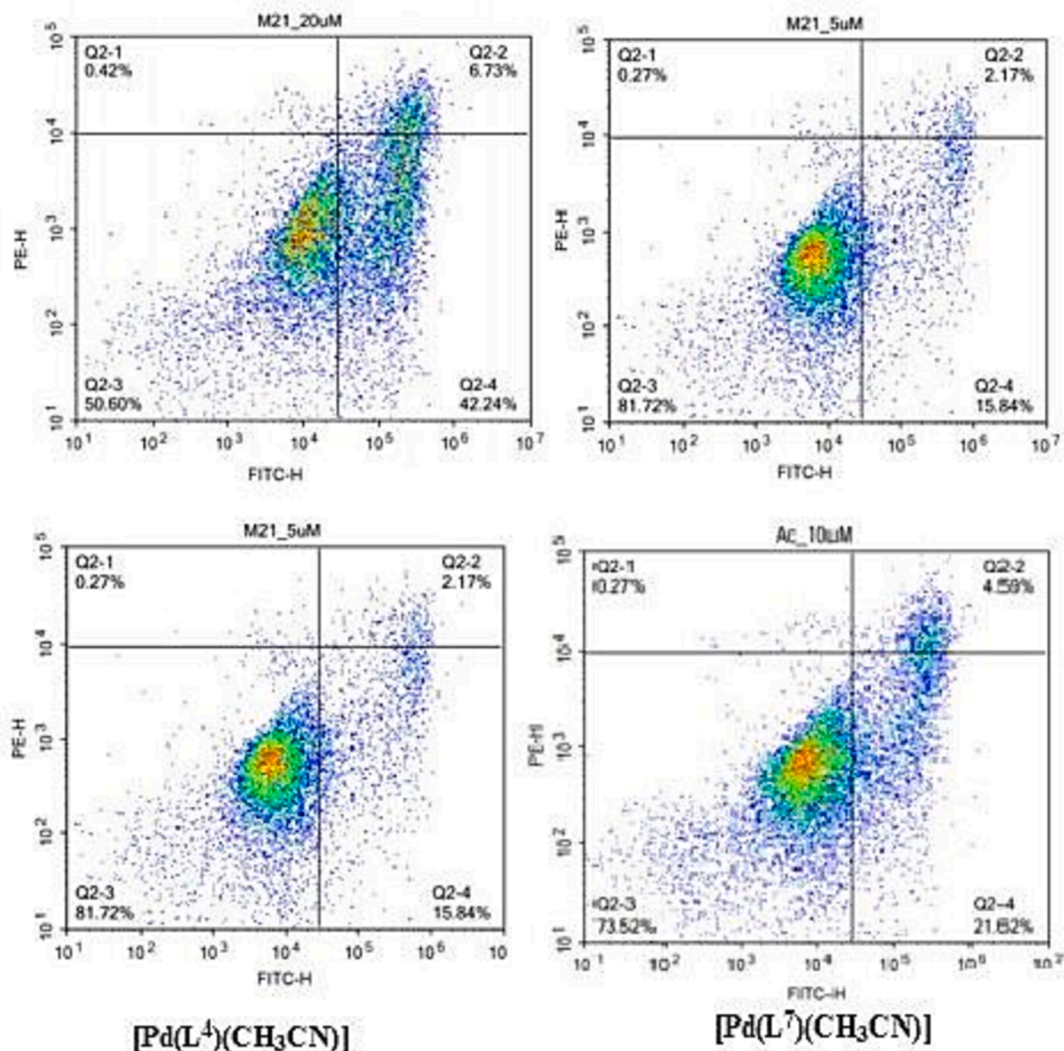
Fig. 7. Cellular apoptosis assessment of four most active complexes.

azomethine carbon for **(H₂L¹-H₂L⁸)** appeared at 164.5–162.7 ppm while other aromatic and aliphatic carbons gave peaks at their characteristic region. In ^{13}CNMR of complexes, the azomethine carbon proligands shifted from 164.5 to 162.7 ppm to 166.5–164.7 ppm in palladium complexes.

In the optimized structure of **[Pd(L⁴)CH₃CN)]**, Pd-N (1.999 – 2.057 A°) and Pd-O (2.025 A°) bonds lengths obtained within acceptable ranges(Zeizinger et al., 2001, Figg et al., 2013). Based on the
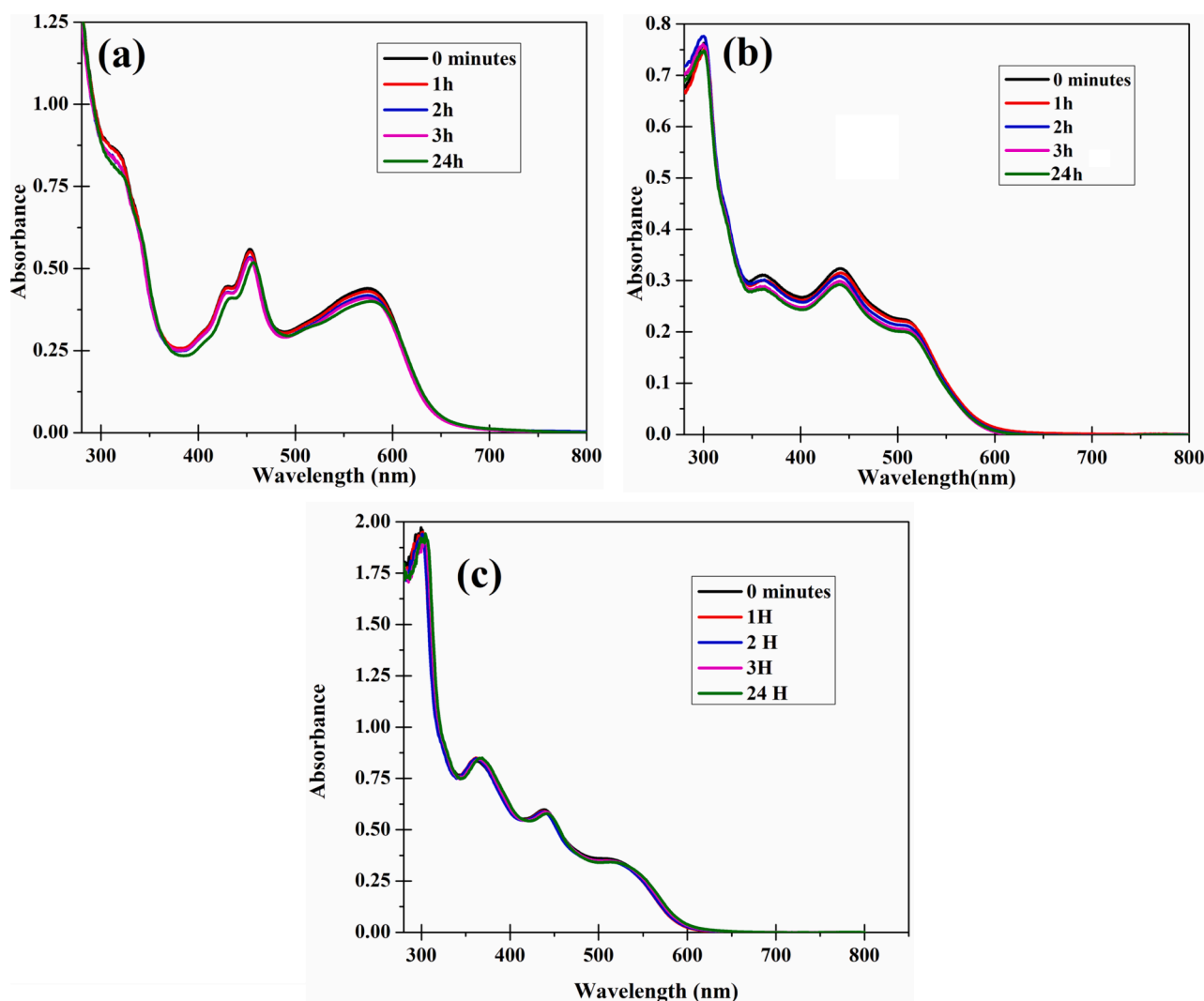
Fig. 8. UV–Vis spectra of **[Pd(L^1)(CH$_3$CN)] (a), [Pd(L^2)(CH$_3$CN)] (b), [Pd(L^3)(CH$_3$CN)] (c)** in DMSO and DI water mixture over a 24 h period.

Table 4
Targeting TKIs: Unveiling potential inhibitors for EGFR, VEGFR, FGFR, HGFR, and SRC.

ID	Docking Score (kcal/mol) (Tyrosine Kinases)				
	EGFR	VEGFR	FGFR	HGFR	SRC
[Pd(L^1)(CH$_3$CN)]	−1.76	−2.17	−1.11	−4.43	−8.66
[Pd(L^2)(CH$_3$CN)]	−7.87	−9.12	−4.98	−7.43	0.00
[Pd(L^3)(CH$_3$CN)]	−5.8	−1.67	−4.31	−7.98	−6.81
[Pd(L^4)(CH$_3$CN)]	−5.99	−7.17	−1.11	−9.98	−6.54
[Pd(L^5)(CH$_3$CN)]	−6.87	−9.81	0.00	0.00	0.00
[Pd(L^6)(CH$_3$CN)]	−2.65	−6.77	0.00	−5.44	−6.66
[Pd(L^7)(CH$_3$CN)]	−6.41	−7.12	−7.79	−6.41	−8.11
[Pd(L^8)(CH$_3$CN)]	−6.53	−5.34	−5.89	−5.53	−4.99

Docking scores are numerical values obtained from molecular docking simulations and are used to assess the binding affinity or potential of a ligand (drug) to a target protein. lower docking scores (more negative values) suggest stronger binding affinity, while higher docking scores (less negative values) indicate weaker binding.

computational study of complex **[Pd(L^4)CH$_3$CN)]**, the calculated HOMO–LUMO band gap was equal to 2.864 eV while the associated energies with each HOMO and LUMO were found to be −4.855 and −1.991 eV respectively. The atomic orbital components of the frontier molecular orbital are shown in Fig. 5. The ability of compounds to donate or receive electrons can be measure from the energies associated

HOMO and LUMO. The molecules with higher E$_{HOMO}$ have greater electron donating ability while the molecules with lower E$_{LUMO}$ show smaller resistance in electrons acceptance (Mansour, 2013, Zeyrek et al., 2015).

Results of the MTT assay revealed that all metal complexes showed potent activity against both cells compared to their respective proligand and precursor. Notably, **[Pd(L^1)(CH$_3$CN)]** was most active amongst all the complexes and showed the IC$_{50}$ value of (25.50 ± 0.3 μM) and (20.76 ± 0.30) against MDA-MB-231 and MCF-7 cell lines respectively.

To determine whether the cytotoxic effects of the synthesized compounds were selective for malignant cells in comparison to nonmalignant cells, the non-tumorigenic MCF-10A cells were exposed to the compounds at varying concentration (5 μM, 10 μM, 25 μM, and 50 μM) in a similar manner as the cancer cells. After MTT assay the results of percent inhibition for MDA-MB-231, MCF-7 and MCF-10A cell lines by metal complexes **[Pd(L^1)(CH$_3$CN)] – [Pd(L^8)(CH$_3$CN)]** are presented in Fig. 6. The results showed that these cells were less susceptible to the actions of the compounds, particularly to the metal complex **[Pd(L^1)(CH$_3$CN)]** that showed more cell death in breast cancer cells.

Data in this study revealed that the triple negative MDA-MB-231 and MCF-7 cells, which bear an aggressive phenotype, responded more favorably to most of the metal complexes and showed greater cytotoxicity. The diminished cytotoxicity observed when non-tumorigenic MCF-10A cells were exposed to compounds **[Pd(L^1)(CH$_3$CN)] – [Pd(L^8)(CH$_3$CN)]** suggested that these novel metal complexes will offer

promising treatment/therapy for patients with breast cancer.

In apoptotic assay, remarkably all compounds displayed the ability to induce apoptosis. Notably, the compound **[Pd(L^1)(CH$_3$CN)]** stood out for its exceptional apoptotic induction capacity. The intriguing aspect lies in its concurrent strong docking affinity and demonstrated anti-cancer activity. This convergence of attributes underscores its potential as a multifaceted candidate with promising implications for therapeutic interventions in breast cancer management. In Fig. 7, we visualize the evaluation of cell apoptosis for the tested compounds through the utilization of the Dead Cell Apoptosis Kit in conjunction with Annexin V FITC and propidium iodide (PI) staining, as facilitated by flow cytometry. The horizontal x-axis on the plot represents the extent of FITC-Annexin V staining, while the vertical y-axis represents the magnitude of PI staining, both displayed in logarithmic units. Cells that find themselves in the early stages of apoptosis are localized within the lower right (LR) quadrant of the dot or density plot. As apoptotic processes commence, Annexin V FITC binding becomes prominent, resulting in an identifiable cluster in this region. Cells residing in the upper right (UR) quadrant represent instances of late apoptotic phenomena. In this segment of the plot, both FITC-Annexin V and PI staining are pronounced, suggesting cells that have progressed further into apoptosis. Conversely, the lower left (LL) quadrant accommodates normal viable cells. Within this area, the absence of strong FITC-Annexin V or PI staining implies cells that have maintained their viability and have yet to engage in apoptosis. This figure provides insights into the apoptotic behavior of the compounds under investigation, offering a comprehensive depiction of cell fate across various stages of apoptosis through distinct quadrants within the dot or density plot. Further interpretation of the data assists in understanding the impact of the tested compounds on cellular processes and viability. The apoptosis of rest four compounds is shown in supporting information **(Figure S25)**.

Among the tested compounds, **[Pd(L^1)(CH$_3$CN)]** emerged as the most promising candidate with the highest overall score **(381.735)**, closely followed by **[Pd(L^2)(CH$_3$CN)]** **(370.506).** These top-ranked compounds demonstrated favorable ADME profiles and strong binding affinity to tyrosine kinases **(Fig. 9)**, suggesting their potential as potent therapeutic agents. Further experimental investigations are necessary to validate their inhibitory activity and pave the way for targeted drug development against tyrosine kinases, particularly in the context of cancer and other related diseases (Al-Janabi et al., 2023).

In the realm of chemical research, the quest for innovative compounds with potent anti-cancer properties has been a driving force, particularly in the field of coordination chemistry (García-Valdivia et al., 2021). In this context, the utilization of Density Functional Theory (DFT) as a crucial tool for understanding and designing novel compounds has gained substantial significance (Deghady et al., 2021). The

pivotal role of DFT calculations lies in their ability to predict and elucidate fundamental properties of molecules and materials, providing invaluable insights into their behavior at the molecular level (Van Mourik et al., 2014). These insights are pivotal for the rational design of new compounds, especially when addressing the pressing issue of translating *in vitro* efficacy to *in vivo* applications (Huo et al., 2021). The study at hand presents a novel series of NNO tridentate ligands that create unique imino, amido, and oxo donor pockets, facilitating Pd(II) coordination. This innovative approach brings forth a new class of compounds that holds great potential as anti-cancer agents. The importance of DFT in this research becomes apparent as it is used to comprehensively understand the electronic and structural properties of these compounds. DFT calculations provide a robust foundation for exploring the mechanistic basis of their anti-cancer effects, guiding the design and development of compounds with enhanced therapeutic potential (Van Mourik et al., 2014, García-Valdivia et al., 2021). The significance of this study is further underscored by the recurrent issue faced by many complexes - the inability to transition effectively from *in vitro* to *in vivo* applications (Deghady et al., 2021). Numerous compounds have demonstrated impressive efficacy in *in vitro* studies but failed to perform optimally in the complex biological environment of *in vivo* systems (Huo et al., 2021). This divergence raises a critical concern that our research aims to address. By employing DFT calculations and molecular docking studies, we seek to bridge the gap between *in vitro* and *in vivo* properties, shedding light on the electronic and structural factors that influence a compound's performance in a biological context. In addition to the promising potential of these compounds, we also aim to emphasize their novelty. The synthesized palladium complexes, characterized meticulously by elemental analysis and advanced spectroscopic techniques, present a compelling perspective on the development of potent anti-cancer agents. The innovative synergy between ligands and Pd(II) complexes opens new avenues for future cancer therapy endeavors.

In computational Assessment for Tyrosine Kinase Inhibitors, the HL^1 and HL^2 were the most active compounds having IC$_{50}$ values of 75.0 ± 0.2 (MDA-MB-231) and 81.6 ± 0.6 (MCF-7) among all proligands. This might be due to the benzyl group attached with the amido arm of proligand as it is planar and lipophilic in nature. These kinds of structures show extensive van der Waals and hydrophobic interactions with similar structural moities of the protein binding sites. The binding region for the aromatic ring is a narrow slot compared to bulky cyclohexyl ring that could allowed better fittings with tyrosine kinase enzyme. All the complexes were more active relative to their respective proligands. **[Pd (L^1)(CH$_3$CN)]** and **[Pd(L^2)(CH$_3$CN)]** showed minimum IC$_{50}$ values, (25.50 ± 0.30 μM) and (20.76 ± 0.30 μM) against MDA-MB-231 and MCF-7 cell lines respectively. The higher cytotoxic activity of complexes was due to the generation of conjugated and planner ligand that
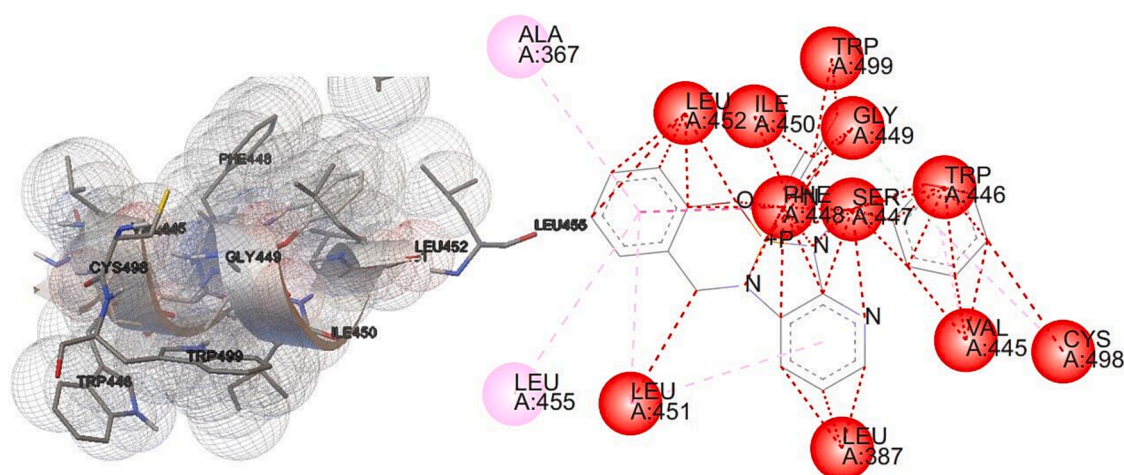

Fig. 9. Putative binding modes and molecular interaction of tyrosine kinases.

chelated with Pd(II) in a square planner geometry. This electron delocalization was extended by the formation of metallo-cycles and additional electrostatic interactions developed with charged bio-metal. Moreover, the labile acetonitrile ligand in palladium(II) complexes could be replace by stronger ligands such as heteroaromatic groups of bioactive substrates, led to a number of cytotoxic mechanisms in the cancer cells (El-Sayed et al., 2021).

5. Conclusions

In this study, novel Pd(II) complexes were synthesized with a series of newly designed NNO tridentate ligands for anticancer studies. The synthesis of these compounds was rigorously confirmed through various analytical techniques, including FTIR, proton and carbon NMR, elemental analysis and single crystal XRD analysis. The structural analysis of the most active complex, **[Pd(L^1)(CH$_3$CN)]**, was also carried out by computational studies. The results of the MTT assay disclosed that all palladium complexes exhibited substantial activity against MDA-MB-231 and MCF-7cells. The complex, **[Pd(L^1)(CH$_3$CN)]**, displayed the highest potency with the respective IC$_{50}$ value of 25.50 ± 0.30 μM and 20.76 ± 0.30 μM against the two breast cancer line lines. Furthermore, molecular docking studies targeting tyrosine kinases, which are recognized as pivotal in cancer, corroborated the anticancer potential of these compounds.

CRediT authorship contribution statement

Shazia Hussain: Formal analysis, Investigation, Visualization, Writing – original draft, Data curation, Validation. **Shabeeb Hussain:** Investigation, Visualization. **M. Naveed Zafar:** Conceptualization, Methodology, Writing – review & editing, Resources, Project administration, Funding acquisition, Supervision. **Irfan Hussain:** Conceptualization. **Faizullah Khan:** Formal analysis. **Ehsan Ullah Mughal:** Methodology. **Muhammad NawazTahir:** Software, Visualization.

Declaration of competing interest

The authors declare that they have no known competing financial interests or personal relationships that could have appeared to influence the work reported in this paper.

Acknowledgments

Appendix A. Supplementary material

^{1}H & ^{13}C NMR, FT-IR spectra of ligand precursors, ligands, and complexes, crystallography details and X-ray crystallographic data in CIF format (CIF). Supplementary data to this article can be found online at https://doi.org/10.1016/j.jsps.2023.101915.

References

Abd El-Halim, H., Mohamed, G.G., Anwar, M.N., 2018. Antimicrobial and anticancer activities of Schiff base ligand and its transition metal mixed ligand complexes with heterocyclic base. Appl. Organomet. Chem. 32, e3899.

Al-Janabi, A.S., Oudah, K.H., Aldossari, S.A., et al., 2023. Spectroscopic, anti-bacterial, anti-cancer and molecular docking of Pd (II) and Pt (II) complexes with (E)-4-((dimethylamino) methyl)-2-((4, 5-dimethylthiazol-2-yl) diazenyl) phenol ligand. J. Saudi Chem. Soc. 27, 101619.

Ambika, S., Manojkumar, Y., Arunachalam, S., et al., 2019. Biomolecular interaction, anti-cancer and anti-angiogenic properties of cobalt (III) Schiff base complexes. Sci. Rep. 9, 2721.

Arjunan, V., Saravanan, I., Ravindran, P., et al., 2009. Structural, vibrational and DFT studies on 2-chloro-1H-isoindole-1, 3 (2H)-dione and 2-methyl-1H-isoindole-1, 3 (2H)-dione. Spectrochim. Acta A Mol. Biomol. Spectrosc. 74, 642–649.

Arpino, G., Wiechmann, L., Osborne, C.K., et al., 2008. Crosstalk between the estrogen receptor and the HER tyrosine kinase receptor family: molecular mechanism and clinical implications for endocrine therapy resistance. Endocr. Rev. 29, 217–233.

Basaran, E., Sogukomerogullari, H.G., Cakmak, R., et al., 2022. Novel chiral Schiff base Palladium (II), Nickel (II), Copper (II) and Iron (II) complexes: Synthesis, characterization, anticancer activity and molecular docking studies. Bioorg. Chem. 129, 106176.

Boshuizen, J., Peeper, D.S., 2020. Rational cancer treatment combinations: an urgent clinical need. Mol. Cell 78, 1002–1018.

Carotti, S., Marcon, G., Marussich, M., et al., 2000. Cytotoxicity and DNA binding properties of a chloro glycylhistidinate gold (III) complex (GHAu). Chem. Biol. Interact. 125, 29–38.

Chohan, Z.H., Sumrra, S.H., 2010. Some biologically active oxovanadium (IV) complexes of triazole derived Schiff bases: their synthesis, characterization and biological properties. J. Enzyme Inhib. Med. Chem. 25, 599–607.

de Miguel, M., Calvo, E., 2020. Clinical challenges of immune checkpoint inhibitors. Cancer Cell 38, 326–333.

Deghady, A.M., Hussein, R.K., Alhamzani, A.G., et al., 2021. Density functional theory and molecular docking investigations of the chemical and antibacterial activities for 1-(4-Hydroxyphenyl)-3-phenylprop-2-en-1-one. Molecules 26, 3631.

Divsalar, A., Saboury, A., Yousefi, R., et al., 2007. Spectroscopic and cytotoxic studies of the novel designed palladium (II) complexes: β-Lactoglobulin and K562 as the targets. Int. J. Biol. Macromol. 40, 381–386.

Divsalar, A., Saboury, A.A., Mansoori-Torshizi, H., et al., 2009. Comparative studies on the interaction between bovine β-lacto-globulin type a and B and a new designed Pd (II) complex with anti-tumor activity at different temperatures. J. Biomol. Struct. Dyn. 26, 587–597.

Divsalar, A., Saboury, A.A., Mansoori-Torshizi, H., et al., 2010. Design, synthesis, and biological evaluation of a new palladium (II) complex: β-lactoglobulin and K562 as targets. J. Phys. Chem. B 114, 3639–3647.

Divsalar, A., Saboury, A.A., Ahadi, L., et al., 2011. Biological evaluation and interaction of a newly designed anti-cancer Pd (II) complex and human serum albumin. J. Biomol. Struct. Dyn. 29, 283–296.

Dorr, R.T., 1996. A review of the modulation of cisplatin toxicities by chemoprotectants. Platinum and other metal coordination compounds in cancer chemotherapy 2, pp. 131-154.

Drilon, A., Siena, S., Ou, S.-H.-I., et al., 2017. Safety and antitumor activity of the multitargeted pan-TRK, ROS1, and ALK inhibitor entrectinib: combined results from two phase I trials (ALKA-372-001 and STARTRK-1). Cancer Discov. 7, 400–409.

Dudani, S., Graham, J., Wells, J.C., et al., 2019. First-line immuno-oncology combination therapies in metastatic renal-cell carcinoma: results from the international metastatic renal-cell carcinoma database consortium. Eur. Urol. 76, 861–867.

Durig, J., Layton, R., Sink, D., et al., 1965. Far infrared spectra of palladium compounds—I. The influence of ligands upon the palladium chloride stretching frequency. Spectrochim. Acta 21, 1367–1378.

Ejidike, I.P., Ajibade, P.A., 2016. Synthesis, characterization, anticancer, and antioxidant studies of Ru (III) complexes of monobasic tridentate Schiff bases. Bioinorganic Chem. Appl.

El-Sayed, W., Alkabli, J., Althumayri, K., et al., 2021. Azomethine-functionalized task-specific ionic liquid for diversion of toxic metal ions in the aqueous environment into pharmacological nominates. J. Mol. Liq. 322, 114525.

Emam, S.M., El Sayed, I.E., Ayad, M.I., et al., 2017. Synthesis, characterization and anticancer activity of new Schiff bases bearing neocryptolepine. J. Mol. Struct. 1146, 600–619.

Ferrari, M.B., Fava, G.G., Leporati, E., et al., 1998. Synthesis, characterisation and biological activity of three copper (II) complexes with a modified nitrogenous base: 5-formyluracil thiosemicarbazone. J. Inorg. Biochem. 70, 145–154.

Figg, T.M., Schoendorff, G., Chilukuri, B., et al., 2013. Structure and bonding of palladium oxos as possible intermediates in metal-carbon oxy insertion reactions. Organometallics 32, 4993–4996.

Gaccioli, F., Franchi-Gazzola, R., Lanfranchi, M., et al., 2005. Synthesis, solution equilibria and antiproliferative activity of copper (II) aminomethyltriazole and aminomethylthioxotriazoline complexes. J. Inorg. Biochem. 99, 1573–1584.

García-Valdivia, A.A., Jannus, F., García-García, A., et al., 2021. Anti-cancer and anti-inflammatory activities of a new family of coordination compounds based on divalent transition metal ions and indazole-3-carboxylic acid. J. Inorg. Biochem. 215, 111308.

Ghani, N.T.A., Mansour, A.M., 2011. Novel Pd (II) and Pt (II) complexes of N, N-donor benzimidazole ligand: Synthesis, spectral, electrochemical, DFT studies and evaluation of biological activity. Inorg. Chim. Acta 373, 249–258.

González, M., Tercero, J., Matilla, A., et al., 1997. Cis-dichloro (α, ω-diamino carboxylate ethyl ester) palladium (II) as palladium (II) versus platinum (II) model anticancer drugs: synthesis, solution equilibria of their aqua, hydroxo, and/or chloro species, and in vitro/in vivo DNA-binding properties. Inorg. Chem. 36, 1806–1812.

Guillen, N., Wieske, M., Otto, A., et al., 2018. Subtractive interaction proteomics reveal a network of signaling pathways activated by an oncogenic transcription factor in acute myeloid leukemia. BioRxiv. 464958.

Huang, L., Jiang, S., Shi, Y., 2020. Tyrosine kinase inhibitors for solid tumors in the past 20 years (2001–2020). J. Hematol. Oncol. 13, 1–23.

Huang, M.-Y., Jiang, X.-M., Wang, B.-L., et al., 2021. Combination therapy with PD-1/PD-L1 blockade in non-small cell lung cancer: strategies and mechanisms. Pharmacol. Ther. 219, 107694.

Huo, C.-M., Chen, L., Wang, H.-Y., et al., 2021. Density functional theory-guided drug loading strategy for sensitized tumor-homing thermotherapy. Chem. Eng. J. 423, 130146.

Hussain, S., Badshah, A., Lal, B., et al., 2014. New supramolecular ferrocene incorporated N, N′-disubstituted thioureas: synthesis, characterization, DNA binding, and antioxidant studies. J. Coord. Chem. 67, 2148–2159.

Hussain, S., Imtiaz-ud-Din, A.R., et al., 2020. New bioactive Cu (I) thiourea derivatives with triphenylphosphine; synthesis, structure and molecular docking studies. J. Coord. Chem. 73, 1191–1207.

Karabacak, M., Asiri, A., Al-Youbi, A., et al., 2014. Identification of structural and spectral features of synthesized cyano-stilbene dye derivatives: a comparative experimental and DFT study. Spectrochim. Acta A Mol. Biomol. Spectrosc. 120, 144–150.

Kostova, I., 2006. Platinum complexes as anticancer agents. Recent Pat. Anticancer Drug Discov. 1, 1–22.

Madhavan, V., Varghese, H.T., Mathew, S., et al., 2009. FT-IR, FT-Raman and DFT calculations of 4-chloro-2-(3, 4-dichlorophenylcarbamoyl) phenyl acetate. Spectrochim. Acta A Mol. Biomol. Spectrosc. 72, 547–553.

Maher, M., Kassab, A.E., Zaher, A.F., et al., 2019. Novel pyrazolo [3, 4-d] pyrimidines: design, synthesis, anticancer activity, dual EGFR/ErbB2 receptor tyrosine kinases inhibitory activity, effects on cell cycle profile and caspase-3-mediated apoptosis. J. Enzyme Inhib. Med. Chem. 34, 532–546.

Makker, V., Rasco, D., Vogelzang, N.J., et al., 2019. Lenvatinib plus pembrolizumab in patients with advanced endometrial cancer: an interim analysis of a multicentre, open-label, single-arm, phase 2 trial. Lancet Oncol. 20, 711–718.

Mandal, S., Tarai, S.K., Pan, A., et al., 2022. Cytotoxic effects of Pd (II) complexes on cancer and normal cells: Their DNA & BSA adduct formation and theoretical approaches. Bioorg. Chem. 128, 106093.

Mansour, A.M., 2013. Coordination behavior of sulfamethazine drug towards Ru (III) and Pt (II) ions: Synthesis, spectral, DFT, magnetic, electrochemical and biological activity studies. Inorg. Chim. Acta 394, 436–445.

Mansouri-Torshizi, H., Mahboube, I., Divsalar, A., et al., 2008. 2, 2′-Bipyridinebutyldithiocarbamatoplatinum (II) and palladium (II) complexes: synthesis, characterization, cytotoxicity, and rich DNA-binding studies. Bioorg. Med. Chem. 16, 9616–9625.

Mansouri-Torshizi, H., Moghaddam, M., Divsalar, A., et al., 2009. Diimine platinum (II) and palladium (II) complexes of dithiocarbamate derivative as potential antitumor agents: synthesis, characterization, cytotoxicity, and detail DNA-binding studies. J. Biomol. Struct. Dyn. 26, 575–586.

Mustafa, G., Zia-ur-Rehman, M., Sumrra, S.H., et al., 2022. A critical review on recent trends on pharmacological applications of pyrazolone endowed derivatives. J. Mol. Struct. 1262, 133044.

Noreen, S., Sumrra, S.H., 2022. Correlating the charge transfer efficiency of metallic sulfa-isatins to design efficient NLO materials with better drug designs. Biometals 35, 519–548.

Oaknin, A., León-Castillo, A., Lorusso, D., 2020. Progress in the management of endometrial cancer (subtypes, immunotherapy, alterations in PIK3CA pathway): data and perspectives. Curr. Opin. Oncol. 32, 471–480.

Obi-Egbedi, N., Obot, I., El-Khaiary, M., et al., 2011. Computational simulation and statistical analysis on the relationship between corrosion inhibition efficiency and molecular structure of some phenanthroline derivatives on mild steel surface. Int. J. Electrochem. Sci. 6, 5649–5675.

Petrović, V.P., Živanović, M.N., Simijonović, D., et al., 2015. Chelate N, O-palladium (II) complexes: synthesis, characterization and biological activity. RSC Adv. 5, 86274–86281.

Rudbari, H.A., Kordestani, N., Cuevas-Vicario, J.V., et al., 2022. Investigation of the influence of chirality and halogen atoms on the anticancer activity of enantiopure palladium (ii) complexes derived from chiral amino-alcohol Schiff bases and 2-picolylamine. New J. Chem. 46, 6470–6483.

Sakhi, M., Khan, A., Iqbal, Z., et al., 2022. Design and characterization of paclitaxel-loaded polymeric nanoparticles decorated with trastuzumab for the effective treatment of breast cancer. Front. Pharmacol. 13, 855294.

Seghir, I., Nebbache, N., Meftah, Y., et al., 2019. DFT/TDDFT Investigation on the Electronic Structure and Spectroscopic Properties of Cis-Dioxomolybdenum (VI) Complexes. Acta Chim. Slov. 66.

Simović, A.R., Masnikosa, R., Bratsos, I., et al., 2019. Chemistry and reactivity of ruthenium (II) complexes: DNA/protein binding mode and anticancer activity are related to the complex structure. Coord. Chem. Rev. 398, 113011.

Sumrra, S.H., Hanif, M., Chohan, Z.H., 2015. Design, synthesis and in vitro bactericidal/fungicidal screening of some vanadyl (IV) complexes with mono-and di-substituted ONS donor triazoles. J. Enzyme Inhib. Med. Chem. 30, 800–808.

Sumrra, S.H., Zafar, W., Javed, H., et al., 2021. Facile synthesis, spectroscopic evaluation and antimicrobial screening of metal endowed triazole compounds. Biometals 34, 1329–1351.

Sumrra, S.H., Mushtaq, F., Ahmad, F., et al., 2022a. Coordination behavior, structural, statistical and theoretical investigation of biologically active metal-based isatin compounds. Chem. Pap. 76, 3705–3727.

Sumrra, S.H., Zafar, W., Imran, M., et al., 2022b. A review on the biomedical efficacy of transition metal triazole compounds. J. Coord. Chem. 75, 293–334.

Tadele, K.T., Tsega, T.W., 2019. Schiff Bases and their metal complexes as potential anticancer candidates: a review of recent works. Anti-Cancer Agents Med. Chem. (formerly Current Medicinal Chemistry-Anti-Cancer Agents) 19, 1786–1795.

Van Mourik, T., Bühl, M., Gaigeot, M.-P., 2014. Density functional theory across chemistry, physics and biology. The Royal Society Publishing.

Welsh, J., 2013. Animal models for studying prevention and treatment of breast cancer. Animal models for the study of human disease, Elsevier, pp. 997-1018.

Zafar, M.N., Masood, S., Muhammad, T.S.T., et al., 2019. Synthesis, characterization and anti-cancer properties of water-soluble bis (PYE) pro-ligands and derived palladium (II) complexes. Dalton Trans. 48, 15408–15418.

Zafar, M.N., Butt, A.M., Perveen, F., et al., 2021. Pd (II) complexes with chelating N-(1-alkylpyridin-4 (1H)-ylidene) amide (PYA) ligands: Synthesis, characterization and evaluation of anticancer activity. J. Inorg. Biochem. 224, 111590.

Zeizinger, M., Burda, J.V., Šponer, J., et al., 2001. A systematic ab initio study of the hydration of selected palladium square-planar complexes. a comparison with platinum analogues. Chem. A Eur. J. 105, 8086–8092.

Zeyrek, C.T., Ünver, H., Arpacı, Ö.T., et al., 2015. Experimental and theoretical characterization of the 2-(4-bromobenzyl)-5-ethylsulphonyl-1, 3-benzoxazole. J. Mol. Struct. 1081, 22–37.

Zhang, Q., Zhong, W., Xing, B., et al., 1998. Binding properties and stoichiometries of a palladium (II) complex to metallothioneins in vivo and in vitro. J. Inorg. Biochem. 72, 195–200.